Significance of direct and indirect radiative forcings of aerosols in the East China Sea region

Teruyuki Nakajima[1†], Miho Sekiguchi[1], Toshihiko Takemura[2], Itsushi Uno[2], Akiko Higurashi[3], Dohyeong Kim[4], Byung Ju Sohn[4], Sung-Nam Oh[5], Takashi Y. Nakajima[6], Sachio Ohta[7], Itaru Okada[8], Tamio Takamura[8], and Kazuaki Kawamoto[9]

[1]Center for Climate System Research, The University of Tokyo,
4-6-1 Komaba, Meguro-ku, Tokyo 153-8904, Japan

[2]Research Institute for Applied Mechanics, Kyushu University, Kasuga Park 6-1,
Kasuga 816-8580, Fukuoka, Japan

[3]Atmospheric Environment Division, National Institute for Environmental Studies,
16-2 Onogawa, Tsukuba, Ibaraki 305-8506, Japan

[4]School of Earth and Environmental Sciences, Seoul National University,
Seoul, 151-747, Korea

[5]Korean Meteorological Research Institute, KMA, Seoul, Korea

[6]NASDA/EORC, 1-8-10 Harumi, Chuo-ku, Tokyo 104-6023, Japan

[7]Division of Environment and Resource Engineering, Graduate School of Engineering,
Hokkaido University, Sapporo 060-8628, Japan

[8]Center for Environmental Remote Sensing, Chiba University,
1-33 Yayoi-cho, Inage-ku, Chiba 263-8522, Japan

[9]Research Institute for Humanity and Nature, Kamigyo-ku, Kyoto 602-0878, Japan

Submitted to the special issue of ACE-Asia, *J. Geophys. Res.*
(November 30, 2002), Revised (April 28, 2003)

[†]Corresponding author (teruyuki@ccsr.u-tokyo.ac.jp)

Abstract

Radiative forcings of aerosols and clouds in the East China Sea region are studied using data from surface radiation measurements, satellite remote sensing, and model simulation conducted in April 2001 as a study of Asian Atmospheric Particle Environmental Change Studies (APEX) cooperating with IGAC/ACE-Asia project. The monthly mean whole sky radiative forcing of the aerosol direct effect is derived from various methods as -5 to -8 W/m^2 at the top of atmosphere (TOA) and -10 to -23 W/m^2 at the earth's surface of Gosan (33.28N, 127.17E) and Amami-Oshima (28.15N, 129.30E) sites, though there is a large regional difference caused by changes in the aerosol optical thickness and single scattering albedo. The cloud forcing is estimated as -20 to -40 W/m^2, so that the aerosol direct forcing can be comparable to the cloud radiative forcing at surface. However the estimate of the aerosol direct forcing thus obtained strongly depends on the estimation method of the aerosol properties, especially on the single scattering albedo, generating a method difference about 40%. The radiative forcing of the aerosol indirect effect is roughly estimated from satellite method and SPRINTARS model as -1 to -3 W/m^2 at both TOA and surface.

1. Introduction

The continental scale air pollution in Asia has drawn a strong attention in recent years from the atmospheric and climate research communities in the context of the global warming and environmental change issues [e.g., IPCC, 2001], because of its large but uncertain climate forcing. One of important interests is that this region has become one of the world's large industrial sectors in the last three decades and is thought to continue growing in this century. The research issues include characterization of the complex airmass with man-made aerosols and mineral dust particles called *Kosa* [Uematsu et al., 2002], radiative forcing evaluation with their strong absorption [Jacobson, 2001a; Takemura et al., 2001], significant aerosol and cloud interaction [Nakajima et al., 2001; Bréon et al., 2002], and precipitation change due to absorbing aerosols [Menon et al., 2002]. There have been several projects planned for studying the aerosol characteristics and its climate effect, such as INDOEX [Ramanathan et al., 2001] and IGAC/ACE-Asia [Huebert, 2003] that are large-scale comprehensive projects to study these issues

covering South and East Asian regions, respectively. Asian countries also have their own national projects with variety of topics depending on the needs and interests in each country. The CREST (Core Research for Evolutional Science and Technology) program of JST (Japan Science and Technology Corporation) has two projects, VMAP (Variability of Marine Aerosol Properties) [Matsumoto et al., 2003] and APEX (this paper), aiming at studies of regional aerosol effects in the East Asian region. APEX (Asian Atmospheric Particle Environmental Studies) has been initiated in 1999 as a five year project for studying the radiative forcing and precipitation changes caused by man-made aerosols in this region. They had two regional experiments, APEX-E1 and E2 experiments, in the eastern part of the East China Sea in December 2000 and April 2001. The latter experiment was cooperated with the ACE-Asia experiment. The main purpose of this paper is to study the radiative forcing caused by aerosols and clouds in this region using various observation data and model simulation results obtained in the APEX-E2 campaign.

The APEX-E2 experiment had activities of ground-based measurements, ferry boat measurements, aircraft measurements with the CSIRO/ARA B200 research aircraft, as well as satellite remote sensing and model simulation of radiation, aerosol and cloud characteristics. Details of each activity will be reported in other papers. Figure 1 and Table 1 show surface sites in Asia useful for the present study. SKYNET is a radiation network implemented with pyranometer and sun/sky photometer called a PREDE skyradiometer maintained by the university community and supported by MEXT (Ministry of Education, Culture, Sports, Science and Technology of Japan), NASDA (National Space Development Agency of Japan) and APEX. Some of Korean and Japanese sites serve as sites of NASA/AERONET [Holben et al., 2001] with CIMEL sunphotometer. ADEC (Aeolian Dust Experiment) is another project implementing a network of skyradiometer, lidar and aerosol sampling. This study uses data from skyradiometers and pyranometers at Gosan and Amami-Oshima (Amami in short). Resulted radiative forcing from the analysis of the data is further compared with results from satellite remote sensing and model simulation to assess an estimate range of the direct and indirect forcings of aerosol in this region. Such detailed comparison of results from various methods are needed especially in the Asian region, because there are no enough research effort to establish well-recognized standard models and satellite remote sensing methods, that suitably reproduce the aerosol properties and radiative forcing in

this region, to be shared in the research community.

2. Aerosol characteristics in the East China Sea region

Evaluation of the aerosol radiative forcing (ARF hereafter) needs aerosol optical parameters, such as aerosol optical thickness (AOT) and single scattering abledo (SSA hereafter), amounts of various level clouds, and cloud optical parameters (Fig. 2).

In this study we use aerosol parameters obtained by the PREDE skyradiometer which measures spectral direct solar irradiances and diffuse sky radiances at wavelengths of λ= 315, 400, 500, 670, 870, 940, and 1020 nm. Data are analyzed by the inversion package, *SKYRAD.pack* version 3, which is an improved version of the algorithm of Nakajima et al. [1996a] with a new routine to derive the real and imaginary parts of the aerosol complex refractive index similar to the algorithm by Dubovik and King [2000]. Kim et al. [2003] applied the algorithm to data from SKYNET sites to derive AOT, size distribution and complex refractive index, and further calculated the downward diffuse and direct broadband shortwave radiative fluxes in clear sky condition to compare with corresponding fluxes measured by Kipp&Zonen CM21 pyranometer and CH-01 pyrheliometer. The skyradiometer has been calibrated by the improved Langley method at each site [Tanaka et al., 1986; Nakajima et al., 1996a]. Our experience on the calibration method indicates the calibration error is less than 2% in the calibration constants of the radiometer. The calibration of the flux radiometer CM21 as the secondary standard pyranometer has a similar accuracy (2%).

Kim et al. [2003] retrieved AOT from two methods, i.e., a standard sunphotometry using the spectral direct solar irradiance for retrieving AOT and an inversion of combined data of optical thickness and spectral sky radiances for retrieving AOT, complex refractive index of aerosols, and size distribution. The latter method has a better performance for retrieving very small AOT. Comparison of two AOT values from direct sunphotometry and sun/sky inversion method indicates some error in the calibration constant of the skyradiometer located in Amami. So, we use in this paper AOT values from sun/sky inversion. Overall accuracy of AOT is less than 0.02 both at Gosan and Amami for all the range of measured AOT. They further retrieved the imaginary index of refraction of aerosols so as to minimize the difference between

theoretical and observed fluxes, as in the diffuse to direct method of King and Herman [1979] and Nakajima et al. [1996b]. We confirmed this imaginary index of refraction is generally close to that retrieved from sun/sky inversion method. Therefore, we use this complex refractive index from the diffuse to direct method along with AOT and size distribution from the sun/sky inversion for evaluation of SSA and ARF. Root mean square deviations (RMSD) in SSA values between two algorithms (the original sun/sky inversion method and the present method) are 0.06 at Gosan and 0.08 at Amami-Oshima. This method is hereafter referred to as *Surface method*.

Another method, referred to as *Satellite method*, for evaluating aerosol optical parameters and ARF in this study uses satellite-received radiances in channel 1 (412nm), 2 (443nm), 6 (670nm), and 8 (865nm) of NASA SeaWiFS satellite-borne imager with the aerosol classification algorithm of Higurashi and Nakajima [2002]. Three months data were analyzed [Higurashi et al., 2003] to retrieve abundance distributions of the four type aerosols, such as sulfate, carbonaceous, mineral dust, and sea salt aerosols, though these types should be regarded as satellite-radiance effective aerosol types, not as chemical aerosol types, respectively representing small-size non-absorbing, small-size absorbing, large-size absorbing, and large-size non-absorbing aerosols. We calculate the aerosol optical parameters for four aerosol types with the corresponding built-in aerosol models in the radiative transfer code *Rstar*, developed in the University of Tokyo, which are based on the WCP aerosol models [WCP, 1983] other than carbonaceous aerosol. The carbonaceous type is defined as an internally mixture of the WCP water soluble substance and soot substance by dry volume fractions of 97% and 3%, respectively. Mono-modal log-normal volume size distribution is assumed:

$$dV/d\ln r = C \exp\{-[\ln (r/r_m)/\ln \sigma]^2/2\}, \qquad (1)$$

with mode radius of $r_m = 0.2\mu$m for sulfate and carbonaceous aerosols and 3 μm for the dust aerosol and dispersion of σ= 2.2. Then the extinction and scattering cross sections of each species are calculated by Mie theory after hygroscopic growth calculation in the meteorological condition at each location obtained from ECMWF objective analysis data. Optical constants of the aerosol mixture are calculated by externally mixing these aerosol types with weights of AOT contributions obtained from the satellite type classification. By this procedure we had several trial calculations to tune evaluated

values to SSA from the surface method and found that the key tuning parameters are soot fraction for the carbonaceous aerosols and mode radius of mineral dust aerosols as tuned as above using surface data from Gosan and Amami-Oshima sites. The total AOT at λ= 500nm is then adjusted to the AOT retrieved from satellite. We have subtracted 0.12 from original values of satellite-retrieved AOT, because a scatter plot between original satellite values and surface-measured values from sun/sky photometers has an offset of 0.12 [Higurashi et al., 2003]. Such offset can be caused by cloud contamination, radiometric calibration error, surface whitecap correction error and so on. Especially we think a large cloud contamination can be caused by our cloud screening algorithm without infrared channels of SeaWiFS sensor. And Gosan site may have some effect from water leaving radiance.

Figure 3 shows the monthly mean AOT at wavelength of 500nm in April 2001 along the longitude of 128°E passing near Amami-Oshima and Gosan sites as a function of latitude. Shown in the figure are four profiles of the total AOT evaluated from surface method, satellite method and two aerosol models, i.e., CCSR/NIES GCM (General Circulation Model) coupled with SPRINTARS aerosol chemical transport model [Takemura et al., 2000] and CFORS meso-scale chemical model [Uno et al., 2003]. The figure also shows AOT for four aerosol types (mineral dust, sulfate, carbonaceous, and sea salt types) from the latter three methods. General features of these AOT profiles resemble each other, though there are several noticeable differences. Firstly the total AOT from CFORS model is smaller by about 0.1 than values from other methods at Gosan site. Secondly the latitudes of the maximum AOT for sulfate and carbonaceous aerosols largely depend on estimation methods. The sulfate maximum is located around 25°N to 30°N with SPRINTARS and around 40°N with CFORS, while the carbonaceous maximum is as high as 37°N with SPRINTARS and as low as 30°N with CFORS. Although the maximum latitude of AOT for carbonaceous aerosol from the satellite method is similar to that of SPRINTARS, the magnitude of the satellite value is larger than the model value. On the other hand, AOT of the sulfate-type aerosol is seriously underestimated by the satellite method as compared with model values. These features in the satellite result are explained by the fact that the satellite algorithm cannot distinguish non-absorbing sulfate aerosol from absorbing carbonaceous aerosol when the loading of the latter aerosol type becomes large. Another difference in the satellite result from the model results is the large AOT of the sea salt type aerosol all over the

latitudes. Cloud contamination is the most possible reason for the large values, since cloud particles can be classified as large non-absorbing particles similar to the sea salt type. One other speculation to explain this phenomenon is that the satellite algorithm mistakenly classifies accumulation mode particles as sea salt type aerosol when they grow in the humid warm atmosphere up to size larger than 0.5 μm in radius at which the Ångström exponent and SSA approach 0 and 1, respectively. If this phenomenon is popular in the maritime atmosphere, the original satellite algorithm needs to be modified to take into account such cases for aerosol classification. Further validation studies should be taken to decrease these differences as discussed.

Figures 4 and 5 show time series of aerosol optical parameters at 500nm estimated from four methods at Gosan and Amami sites. Here the asymmetry factor, g, is also shown in the figures because this parameter is important for evaluating the radiative flux,

$$g = < \cos\Theta \ P(\Theta) > / < P(\Theta) >, \qquad (2)$$

where $P(\Theta)$ is the aerosol scattering phase function at scattering angle Θ and $< >$ indicates the angular integration operation in terms of cos Θ. Satellite data have been averaged in 3 degree by 3 degree box around the observation sites in order to filter the small-scale variation and noises in the satellite product. It is found that the time variation in the parameters correlate among the results from various methods, though there are off-phase differences, even between the two model results, suggesting the exact timing of large AOT events is difficult to be simulated by models. Satellite-retrieved AOT tends to reach a value larger than those from other methods, such as on 5, 6, and 13 April at Gosan. SSA from the surface method on 9 and 19 April at Gosan, and 9 and 22 April at Amami are significantly lower than those from other methods. This very low SSA values may reflect the real situation in some extent as discussed below regarding Fig. 7, but we suspect an underestimation of SSA due to instability or error in the inversion of skyradiometer data and diffuse/direct method. Such instability can be possible because the information content of SSA in the radiance data is very small. The low asymmetry factor around 0.66 from 12 to 19 April at Gosan may be true signals because this period had a large Kosa event as shown by the small asymmetry factor at Amami-Oshima. The surface data also support such low asymmetry factor at Gosan.

Taking into account the off-phase features in the time series in Figs. 4 and 5, we take a simple monthly mean average, rather than a scatter plot, for quantitative comparison of AOT, SSA, and asymmetry factor from various methods as shown in Fig. 6 and Table 2. In the figure we show three groups for comparison, i.e., averages of all available daily mean values at the two sites and averages of data on 7 days at Gosan and 5 days at Amami-Oshima when all the four method results are available. The figure indicates AOT agrees with each other 0.1 and SSA within 0.03. The asymmetry factor takes a mean value of 0.70 from all the methods both at Gosan and Amami-Oshima without much variability. There are, however, several differences to be noted. First of all AOT from models tends to be smaller than those from satellite and surface methods, especially at Gosan where the CFORS value is smaller by 0.14 than that from the satellite method. SSA from the surface method is smaller by 0.1 than that from the satellite method at Amami. This small SSA value comes from the very low SSA on several days in the time series of SSA in Fig. 5.

Another important point in Fig. 6 is that there is a noticeable clear-sky bias only in the model results when the good clear sky condition is established in which the surface and satellite methods were available, suggesting a modeling problem in the simulation of low AOT in the strong high pressure condition. Apart from this bias, there is no significant difference in the statistics in the three groups in terms of agreement among the methods, indicating that we can use the monthly value of all daily mean values at Gosan and Amami for further evaluation of ARF.

The small SSA values at Amami-Oshima site evaluated by the surface method were also observed by absorption photometer (Radiance Research PSAP) and TSI nephelometer as shown in Fig. 7 [Ohta et al., 2002]. The SSA from PSAP and nephelometer ran in a range between 0.8 and 1. It became as low as 0.8 when mineral dust particles prevailed over Amami-Oshima in a large Kosa event from 11 to 16 April as indicated by the increased dust concentration in the chemical composition. We should note that this low SSA is contrary to the recent suggestion of large SSA values as ω= 0.95 [Nakajima et al., 1989; Kaufman et al., 2002], suggesting that the contribution of man-made aerosols simultaneously transported from the continent is important to reduce the SSA at Amami-Oshima. This suggestion is supported by large concentrations of organic and black carbon aerosols observed in this period as also shown in the figure. Furthermore Takemura et al. [2002b] proposed AOT of man-made aerosols is larger

than that of mineral dust aerosols even in the large Kosa events in 2000 and 2001. With such low SSA values in the dust event, the April mean SSA value from PSAP/nephelometer becomes as small as 0.85 to 0.88. Although this SSA range is larger than the surface method value, consistent with the April mean of 0.86 in Table 2 from the surface method. Thus, we cannot discard the possibility that the SSA from the models and satellite method are overestimated by about 0.05. This expectation is also suggested Takemura et al. [2002a] who found an overestimation of SSA of fine aerosol particles by 0.02 as compared with ground-truth values from AERONET.

AOT and SSA at locations listed in Table 1 are calculated as in Fig. 8 to see the spatial distributions of these aerosol parameters. The figure indicates that surface-measured AOT is in accord with the satellite at Gosan and Amami-Oshima as already studied in Fig. 6. The satellite-derived AOT becomes large at sites near the continent, while it approaches those from other methods at the remote sites. The model results are generally smaller than the satellite results with very weak site dependence, though SPRINTARS model values follow the satellite and surface values in a better way than CFORS result. This tendency is consistent with the modeled AOT of small size aerosols is widely distributed over the entire region of the East China Sea as also shown in Fig. 3. SSA values shown in Fig. 8 are similar to each other by difference less than 0.05, other than Amami site with a large difference as 0.1 between surface and other methods.

Although we found some differences among the optical parameters derived as above, we will use these data sets to generate ARF to investigate the ARF range in the East China Sea region evaluated by several methods. It will be useful to study the relation between uncertainties in aerosol parameters and ARF when we use one of these methods for estimating the radiative properties of the East Asian atmosphere.

3. Radiative forcing of the aerosol direct effect

This study adopts a flow of radiative forcing evaluation as in Fig. 2 utilizing data from skyradiometer, pyranometer, pyrheliometer, and satellite data. The most direct method of evaluating ARF, which is referred to as *Surface method*, is a method of using only site data. Instantaneous shortwave diffuse and direct radiative fluxes are calculated from aerosol size distribution and SSA inverted from skyradiometer, and are compared

with the measured values with pyranometer and pyrheliometer. Such comparison gives an optimum complex refractive index of aerosols and SSA value consistent with both spectral sun/sky radiances and diffuse/direct broadband radiative fluxes. This aerosol model is further used to theoretically evaluate the shortwave 24 hour mean clear sky net shortwave ARF as labeled *ARF*(*SW*,*clr*) in Table 2. A Lambertian ground surface with ground albedo of 0.1 is assumed in this calculation.

The other method of evaluating ARF, referred as to *Satellite method*, is to use SeaWiFS-derived AOT and aerosol type classification. The broadband radiative fluxes at TOA and surface are calculated by *Rstar*-code using the optical parameters of four type aerosols estimated as in the previous section. Taking account of the lidar measurements [Shimizu et al., 2003], aerosols are loaded in the lowest 2km layers in the atmosphere with temperature and humidity profiles obtained from ECMWF objective analysis data. Ocean surface boundary model [Nakajima et al., 1983] and four stream discrete-matrix method [Nakajima et al., 1986] with Lowtran-7 gas absorption model are used in *Rstar*-code to solve the instantaneous radiative transfer. Shortwave and longwave net radiative forcings are calculated at the top of the atmosphere (TOA) and surface (SFC).

Before studying the detailed values of ARF, let us consider how it depends on the aerosol parameters. The 24 hour mean clear sky net shortwave radiative fluxes at surface, F_{sfc}, and at TOA, F_{toa}, are given in a single scattering and two stream approximation as

$$m R^2 F_{sfc}/SD = (1-A_g)\, t\, T_u/ (1- r A_g)$$
$$\text{and} \quad m R^2 F_{toa} / SD = 1 - T_u{}^2 [r + A_g t^2 / (1- rA_g)], \qquad (3a)$$

where m is the mean optical airmass of the atmosphere which is often given as 1.732 in the two stream Gaussian quadrature approximation; A_g is the ground albedo; S, D, and R are solar constant (approximately 1370 W/m^2), daytime fraction of the day, and earth-sun distrance in astronomical unit; T_u are transimissivity of the atmosphere above the aerosol layer including ozone and water vapor absorption. The spherical reflectivity and transmissivity of the atmosphere, r and t, are given under the present approximation as

$$r = m\omega\tau b \quad \text{and} \quad t = 1 - m(1-\omega f)\, \tau, \qquad (3b)$$

$$f = (1+g)/2 \quad \text{and} \quad b = (1-g)/2, \tag{3c}$$

where τ and ω are total optical thickness and single scattering albedo of the airmass; f and b are forward and backward scattering coefficients calculated from the asymmetry factor g. These aerosol parameters should be regarded as effective values for entire shortwave spectrum to give suitable radiative flux values. Subtracting the corresponding fluxes for the atmosphere without aerosols, we have ARF by neglecting orders of A_g^2 and rA_g as

$$ARF(SW,clr,sfc) = -(1-A_g)(1-\omega_a f_a)\,\tau_a\,T_u SD/R^2,$$
$$\text{and} \quad ARF(SW,clr,toa) = -[\omega_a b_a - A_g(1-\omega_a f_a)]\,\tau_a\,T_u^2 SD/R^2, \tag{3d}$$

where quantities with suffix-a indicate corresponding quantities for aerosols. These equations suggest the clear sky ARF is approximated by a simple form with aerosol optical parameters and ground albedo. Especially ARF at surface is in the following simple formula:

$$ARFN(SW,clr,sfc) = ARF(SW,clr,sfc)/SDR^2 = -\gamma u$$
$$\text{with} \quad u = [1-\omega_{500}(1+g_{500})/2]\,\tau_{500}. \tag{4}$$

Here we define the scaled ARF as *ARFN* and scaled AOT as u. Different from Eq. (3), we use aerosol parameters at a reference wavelength, say 500nm, yielding the wavelength scaling effect to the coefficient γ. Comparing this formula with a traditional one with the forcing efficiency factor β,

$$ARF(SW,clr,sfc) = -\beta\,\tau_{500}, \tag{5}$$

it is found that the forcing efficiency factor β depends on various factors, such as daytime fraction D, SSA and asymmetry factor, whereas the scaled forcing efficiency γ depends mainly on the scaled AOT.

Figures 9 and 10 show two representations of 24 hour mean clear sky net shortwave ARF at surface as a function of the aerosol parameters derived from the surface method at Gosan and Amami-Oshima. Also shown are theoretical curves calculated by

assuming the June aerosol size distribution and US standard atmosphere. In the theoretical calculation we fix the real part of the aerosol refractive index at 1.5 and change the imaginary index of refraction from 0 to -0.05 as indicated in the figure. From Fig. 8 it is found that ARF at Amami-Oshima varied significantly in the observation period covering several constant SSA lines with the β-value ranging from 50 to 110, while ARF at Gosan is relatively confined in the imaginary refractive index range from -0.005 to -0.02 with the β-value around 80. The small SSA value in Fig. 6 is reflected in these ARF differences at the two sites in Fig. 9. From Fig. 10 and also from several numerical test calculations, the representation given by Eq. (4) is very robust to difference in the aerosol optical model and temperature/water vapor profiles. For the entire target period and data from Gosan and Amami-Oshima sites, the γ value takes almost a unique value as γ= 0.40. Assuming R=1 and D= 0.53 (the actual D-value ranges from 0.51 to 0.55 at Gosan and 0.52 to 0.54 at Amami-Oshima depending on day of April), this γ value produces β= 54.9 to 71.3 at Gosan due to one RMSD change in ω and β = 60.0 to 66.1 due to one RMSD change in g around the mean values of the four methods listed in Table 2. The corresponding values at Amami are β = 54.7 to 69.3 due to ω change and β= 58.3 to 65.6 due to g change. In this way the β value is highly dependent on changes in ω and g values. In our surface data, 75% uncertainty in the β-value is caused SSA uncertainty, and 25% is caused by uncertainty in the asymmetry factor depending on the evaluation methods at both Gosan and Amami-Oshima. ARF itself varies about 40% due to change in AOT. If we use the averaged ARF and AOT of the results from the four methods, the β-value becomes 63.9 at Gosan and 62.7 at Amami, suggesting there is no significant differences in the absorptivity of the atmospheres at these sites. It should be noticed, however, that the atmosphere might be more absorptive with β= 79.7 if we take the small SSA as 0.86 from the surface method at Amami-Oshima. As indicated in Fig. 9, the variability in the β value is much larger at Amami-Oshima than at Gosan when we assume the aerosol parameters from the surface method, suggesting the aimass of Amami-Oshima is more complicated by large variation of contributions from different aerosol species.

For whole sky condition calculations, cloud height, optical thickness and temperature are given to low, middle, and high level clouds every hour from JMA (Japan Meteorological Agency) GMS-5 geostationary satellite retrieval at Chiba University [Okada et al., 2002]. Their algorithm adopts the cloud classification method

of the ISCCP algorithm [Rossow et al., 1993] with a cirrus detection algorithm using split window channels of GMS-5. The cloud optical thickness is retrieved from band-1 of GMS-5 by assuming 10 μm effective cloud particle radius and using the algorithm of Kawamoto et al. [2001]. The cloud classification is applied for pixels in every 0.5 degree by 0.5 degree box in the region of 20S-60N and 80E-160E every hour of April 2001. The classified pixels are further used to obtain the cloud fraction of high, middle, and low clouds by using a partial cloud-layering retrieval algorithm. In this study we adopt completely random layering assumption of high, middle, and low level clouds. For the monthly radiative forcing calculation we simply use the atmosphere model obtained by averaging daily atmospheres thus constructed. Whole sky calculation assumes same aerosol vertical distributions and optical properties in the cloud layer with external mixture assumption.

First of all we compare in Fig. 11 and Table 2 the 24 hour clear sky net shortwave ARF at TOA and surface. The mean AOT at TOA is -10.0±4.3 W/m^2 at Gosan and -9.1±3.8 W/m^2 at Amami-Oshima, respectively. These ranges are comparable to or slightly smaller in magnitude than the range from -7 W/m^2 to - 5 W/m^2 derived from AVHRR in the Northern Hemispheric Indian Ocean region proposed by Rajeev and Ramanathan [2001]. On the other hand, ARF at surface takes -24.5±9.7 W/m^2 at Gosan and and -22.8±8.7 W/m^2 at Amami-Oshima. Although the mean values are similar at Gosan and Amami-Oshima, it should be noted that the RMSD value is as large as more than 40% of the mean value. There are systematic differences between ARF evaluated from models and from satellite and surface methods. This difference reaches -10 W/m^2 at surface. Especially ARF at surface takes a large negative value as -30.7 W/m^2 from the satellite method at Gosan and -31.1 W/m^2 from the surface method at Amami-Oshima. These large forcings are attributed to the large AOT and small SSA derived from the satellite method at Gosan and the large SSA from the surface method at Amami-Oshima.

Whole sky net total ARF for aerosol direct effect are shown in Fig. 12 with cloud parameters used in the forcing calculation. Cloud statistics used in the calculation at Gosan and Amami is listed in Table 3. Dependence of ARF on the site location and on the evaluation method has similar features as found in clear sky shortwave cases, though the magnitude is significantly reduced by clouds. The TOA forcing ranges from -5 W/m^2 to -8 W/m^2 except for the large value as -12 W/m^2 at Quindao and Anmyondo

from the satellite method. These sites near the continent have a large AOT as high as 0.6 in the satellite method. The estimate of the surface forcing is more dependent on the estimation methods. The satellite method derives a forcing from -12 W/m^2 to -35 W/m^2 with a tendency of small surface forcing at remote sites due to their small AOT. On the other hand, model simulation yields -11 W/m^2 to -19 W/m^2 reflecting the simulated small AOT values.

Figure 13 shows the horizontal distribution of the aerosol direct forcing simulated by SPRINTARS. Large negative forcing area extends from Chinese coast to Japan Islands.

4. Cloud forcing and indirect effects of aerosols

The cloud radiative forcing (CRF) is calculated as in Fig. 14 using April monthly mean cloud parameters from GMS remote sensing as listed in Table 3 for Gosan and Amami-Oshima. In the calculation the aerosols obtained in the previous section is introduced in the cloud layer by external mixture. Since the cloud layer does not significantly absorb the solar radiation, forcing values are similar at TOA and surface. The figure shows the shortwave forcing is cancelled by the longwave forcing by about 50% producing the net forcing from -10 W/m^2 to -40 W/m^2 at both TOA and surface with site-averaged cloud fractions of 16.9%, 24.7%, and 15.4% for high, middle, and low level clouds, respectively. The range of the cloud forcing is similar to that of the aerosol direct forcing at surface. It is important to recognize that site dependences of the surface aerosol and cloud forcings are opposite in a sense that large aerosol forcing and small cloud forcing occur at northern sites, while small aerosol forcing and large cloud forcing are realized at southern remote sites. This characteristic dependence between aerosol and cloud forcings is caused not only by the obvious cloud fraction effect but also by two independent factors, i.e., large AOT and large longwave cloud forcing at northern sites. It is also important to note that the RMSD value of cloud amount and cloud optical thickness is very large as shown in Table 3. This large variability indicates that CRF can take values largely different from mean values depending day and location. It is, therefore, the impact calculation of the radiative forcing to the climate formation study should be careful to include such variability.

The indirect forcing of aerosols is difficult to be accessed, different from the direct forcing calculation, because the perturbation has to be calculated with and without aerosols. In this process various feedbacks between clouds and aerosols are caused. Especially 2nd kind of indirect effect and semi-direct effect are difficult to be evaluated because these are complicatedly related with cloud formation processes. GCM modeling is doubtful in this sense to simulate such cloud formation processes resulting in a large variety of the estimates among models. If we strictly think about the detailed cloud formation process, zero aerosol condition has no meaning in the simulation by any present-day GCMs or meso-scale models. Therefore, in this paper, we do not intent to derive the indirect forcing with the same accuracy as that of direct aerosol and cloud forcings, but want to show rather a constraint limit for the estimate.

One key parameter for posing a constraint to the magnitude of the aerosol indirect forcing is the effective cloud particle radius which decreases with increasing CCN number when hygroscopic aerosols are provided as a cloud condensation nuclei (CCN). Figure 15 compares distributions of the effective particle radius of low level clouds with cloud top temperature larger than 273K evaluated by MODIS satellite retrievals and SPRINTARS model simulation. T.Y. Nakajima et al. [2003] obtained cloud optical thickness and effective particle radius from visible and 2.2 μm channel radiances of MODIS applying the solar reflection method [Nakajima and Nakajimam, 1995]. The figure shows that the effective particle radius of the low level cloud is small as 10 μm to 12 μm in the East China Sea region as compared with 14 μm to 16 μm outside this region. The observed pattern of low particle region extends from Taiwan to Korean Peninsula regions and the Western Pacific region to the south of the Kyushu Island. This split pattern resembles the aerosol flow pattern generated by the characteristic weather pressure system in this season simulated by CFORS model [Uno et al., 2003]. On the other hand this detailed pattern is vaguely simulated by SPRINTARS model with spatial resolution of T42. Rather the particle size is smaller around the region of Korean Peninsula to Japan Sea than around the region of Taiwan to Amami-Oshima different from the observed feature by the satellite. A meso-scale model has to be used in future for detailed study of this characteristic regional dependence of aerosol-cloud interaction phenomenon.

The indirect forcing evaluation also needs the particle size in the unperturbed condition together with the present distribution. For this purpose we plot a time series of

the effective particle radius at Gosan and Amami-Oshima as in Fig. 16. This time series was derived from AVHRR data from 1985 to 1995 using the solar reflection algorithm of Kawamoto et al. [2001]. Although the observation period does not cover the year 2001, it is interesting to find that the mean particle radius is systematically larger at Gosan than at Amami even consistent with the regional pattern of the effective radius observed by MODIS as shown in Fig. 15. The seasonal variation of the effective particle radius is found to be of order of 2 μm similar to the particle size difference found in Fig. 15. This observation suggests that 2 μm particle size change is a reasonable estimate for particle size change caused by aerosol and cloud interaction in the East China Sea region, although a part of the seasonal change should be attributed to the dynamical effect.

In order to find how much aerosols can cause the cloud particle radius change, we further investigate the four months data of AVHRR-derived aerosol and cloud parameters in the East China Sea region using the method of Nakajima et al. [2001]. This method uses the statistical correlation curve between cloud parameters and the column aerosol number N_a, such as r_e vs $\ln(N_a)$ for effective particle radius case as an example at Gosan and Amami-Oshima. Sekiguchi et a. [2003] extended this method to include correlations of cloud optical thickness τ_c, effective radius r_e, and cloud amount n with N_a. They did not find a significant correlation of cloud top temperature with N_a. The change in the cloud optical thickness $\Delta\tau_c$, effective particle radius Δr_e, and cloud amount Δn can be obtained from a prescribed N_a change, say $\Delta\ln(N_a) = 0.3$ in this study, and these correlation curves. We adopted the monthly mean correlation curve of April 1990 with a 30% change in the column aerosol number of man-made aerosols after the Industrial Revolution following the discussion of Nakajima et al. [2001]. These cloud parameter changes are used to calculate the monthly mean indirect radiative forcing in April 1990 as shown in Fig. 17 and listed in Table 2. The simulated indirect forcing values of man-made aerosols by SPRINTARS model are also shown in the figure and table. In the model calculation we took a forcing difference between with and without East Asian man-made aerosols. Similarity of the results from AVHRR and SPINTARS suggests that the assumption of 30% N_a change is not far from the reality to estimate the anthropogenic aerosol indirect forcing from satellite. As a result, man-made aerosols in the East Asian region are estimated to produce indirect forcing of -0.35 to -0.86 W/m2 at TOA and -1.55 to -1.30 W/m2 at surface of Gosan as an example. Corresponding

particle radius reductions are shown in Fig. 18 which yields a mean value of 0.49±0.43μm. Since the cloud parameters correlate linearly with the logarithm of N_a [Nakajima et al., 2001], an estimate of the indirect forcing of total aerosols will be obtained by multiplying the calculated values for 30% N_a change by a factor 2 to get the forcing values of -0.7 to -1.7 W/m^2 at TOA and -2.6 to -3.1 W/m^2 at surface, at Gosan for example, for 110% increase in N_a including the change by natural aerosols. The corresponding change of the cloud particle radius is about 1 μm which does not contradict with the particle radius change of about 2 μm as found in Figs. 15 and 16.

5. Conclusions

We have studied the radiative forcing caused by aerosols and clouds in the East China Sea region using satellite data, surface data and model simulation. Resulted monthly mean aerosol direct forcing at surface in April 2001 was found to depend by 40% on the estimation methods, since AOT varies from 0.3 to 0.4 and SSA is largely different from 0.86 to 0.95 depending on the methods. Uncertainty in the asymmetry factor also cannot be neglected. The small SSA at Amami-Oshima is also supported by PSAP/nephelometer measurements at Amami-Oshima. These small values in this region were also proposed by other studies [Tanaka et al., 1983; Jacobson, 2001b]. Ramanathan et al. [2001] proposed a SSA range from 0.85 to 0.90 in the INDOEX region. On the other hand, GCM models seem to have a problem to simulate such low SSA values in the East Asian region. Ghan et al [2001] simulated SSA as large as 0.95 in this region. We also had large SSA values from the two models in our study. Kinne et al. [2002] found a large GCM model dependence in simulated AOT fractions of sulfate, carbonaceous, and mineral dust aerosols, which clearly indicates such improper SSA simulation is caused by problems in simulating the complex aerosol mixture near the aerosol sources.

To quantify the atmospheric absorptivity we have evaluated the radiative forcing efficiency β and also scaled efficiency γ. Results produced β= 25 to 26 at TOA and β= 63 at surface of both Gosan and Amami-Oshima, but it reaches 80 if we adopt the low SSA from surface method. Comparing these values with the reported efficiency factors, 30 at TOA and 70 at surface in TARFOX experiment [Russel et al., 1999] and 25 and 75

in INDOEX experiment [Ramanathan et al., 2001], it is found that the atmospheric absorption in the East China Sea region is similar or slightly smaller than those of TARFOX and INDOEX atmospheres.

To conclude this study, we summarize the obtained forcing values at Gosan and Amami-Oshima sites as in Fig. 19. The figure also shows monthly mean values of sensible and latent heat flux evaluated by the JMA/NHM non-hydrostatic meso-scale model [Saito and Kato, 1999]. The cloud forcing at Amami-Oshima is twice larger than that of Gosan mainly because of large low cloud amount and cloud optical thickness. Whole sky net aerosol direct forcing is -5.6±0.9 W.m^2 at Gosan and -7.1±1.5 W.m^2 at Amami-Oshima at TOA, and as large as -15.8±6.6 W.m^2 and -18.2±5.9 W.m^2 at surface. It should be noted that the Amami-Oshima site has a large uncertainty and also large variability (Table 2) in the ARF values due to uncertainty in the retrieved SSA and large variability in SSA from the surface method. This indicates that airmass at Amami-Oshima is very complex to cause large variety. Our values are again similar or slightly smaller to those of Ramanathan et al. [2001], -2.0 W/m^2 at TOA and -16 W/m^2 at surface, in the Indian Ocean region (0° to 20°N; 40°-100°E). In this regard, it is important to understand the effect of mixing condition of aerosols in the cloud layer for the calculation of CRF and ARF. For this purpose, we tentatively double the co-albedo (1- SSA) of the external aerosols included in the cloud layer in order to roughly estimate the enhanced effect of internally mixed soot particles in cloud droplets in the forcing calculation following the discussion of Kaufman and Nakajima [1993]. If we simply define CRF as the difference between whole sky flux and clear sky flux, then this simulation gives us a reduction of the magnitude of CRF by 3.3 W/m2 at TOA and increase of CRF at surface by the same amount as an average of Gosan and Amami results. And if we define ARF as the difference between whole sky fluxes with and without aerosols, then the same amount of change happens in ARF. This amount is the same order of the difference in our results and INDOEX results, so that we should carry more studies in the flux evaluation for cloud-laden atmosphere including investigation of the aerosol mixture condition of in cloud layers.

The indirect forcing of natural and man-made aerosols is evaluated as -1.2±0.7 W/m^2 at Gosan and -3.2±0.1 W/m^2 at Amami-Oshima at TOA. In the AVHRR analysis with the correlation curves of April 1990, we found contributions of 33%, 65% and 2% of the total indirect forcing are caused by 1st (due to change in the effective radius), 2nd

(due to changes of liquid water path), and cloud fraction. Sekiguchi et al. [2003] proposed corresponding contributions of 31%, 44%, and 25% on global average from analysis of the same AVHRR data set we used. The first kind effect looks only one third of the total indirect effects of aerosols in the satellite method. The surface indirect forcing is in same order of the TOA value. These values are significantly smaller than those of Ramanathan et al. [2001], which are -12 W/m^2 at TOA. It should be noted in this regard that the INDOEX value is largely cancelled by semi-indirect effect as +6 W/m^2 at TOA. On the other hand our indirect forcing estimation includes the semi-indirect effect in the GCM calculation and also in the satellite estimation. Since our analysis has a large uncertainty, it will not be suitable to proceed on further discussion other than pointing out that this large indirect forcing seems to contradict to finding of Nakajima et al. [2001] and Sekiguchi et al. [2002] that there is no strong correlation between cloud parameters and column aerosol number for low level clouds with cloud top temperature larger than 257K in the Indian Ocean region. The key issue to solve this contradiction will be aerosol and cloud interaction with deep convective clouds prevailing in the tropical ocean region, which are excluded in our estimation.

Nonetheless the importance of the indirect effect is not decreased by the small values obtained in this study. It should be noted that CCSR/NIES GCM model coupled with SPRINTARS aerosol model produces a global mean TOA indirect forcing of anthropogenic aerosol as about -1 W/m^2, whereas the global mean direct forcing is calculated as small as -0.2 W/m^2 at TOA [Takemura et al., 2003]. The global mean indirect forcing of man-made aerosols is only half of our site-averaged indirect forcing value obtained in this study. This fact suggests that regional indirect forcing can contribute efficiently to the global mean value in a cumulative manner. On the other hand, the large negative regional direct forcing tends to be cancelled by a positive forcing over land in the process of global average. Therefore the aerosol indirect forcing is more effective than direct forcing to change the planetary energy budget at TOA, while the aerosol direct forcing has a strong contribution to redistribution of energy inside the earth-atmosphere system.

It is obvious from the present study that we need further studies to improve our evaluation and understanding on the direct and indirect effects of aerosols in the East Asian region.

Acknowledgments. This work was supported by JST/CREST project. We are grateful to Japan Meteorological Agency and Yuji Maruyama of CCSR for providing JMA/NHM model numerical simulation results. NASA SeaWiFS data were provided from Japan Marine Science and Technology Corporation, and MODIS data were provided from NASA Goddard Space Flight Center.

References

Bréon, F.-M., D. Tanré, and S. Generoso, Aerosols effect on cloud droplet size monitored from satellite, *Science*, **295**, 834-838, 2002.

Charlson, R. J., S. E. Schwartz, J. M. Hales, R. D. Cess, J. A. Coakley, Jr., J. E. Hansen, D. J. Hofmann, Climate forcing by anthropogenic aerosols, *Science,* **25**, 426-430, 1992.

Dubovik, O., and M.D. King, A flexible inversion algorithm for retrieval of aerosol optical properties from sun and sky radiance measurements, *J. Geophys. Res.*, **105**, 20673-20696, 2000.

Ghan, S., N. Laulainen, R. Easter, R. Wagener, S. Nemesure, E. Chapman, Y. Zhang, and R. Leung, Evaluation of aerosol direct radiative forcing in MIRAGE, *J. Geophys. Res.*, 10**6, 5**295-5316, 2001.

Higurashi, A., and T. Nakajima, Detection of aerosol types over the East China Sea near Japan from four-channel satellite data. *Geophys. Res. Lett.*, 29, 1836, doi:10.1029/2002GL015357, 2002.

Higurashi, A., T. Nakajima, T. Takamura, and B. Holben, Aerosol classification from satellite remote sensing in the East Asia, *J. Geophys. Res.*, ACE-Asia Special Issue, submitting, 2003.

Holben, B.N., D. Tanré, A. Smirnov, T.F. Eck, I. Slutsker, N. Abuhassan, W.W. Newcomb, J.S.Schafer, B. Chatenet, F. Lavenu, Y.J. Kaufman, J.V. Castle, A. Setzer, B. Markham, D. Clark, R. Frouin, R. Halthore, A. Karneli, N.T. O'Neill, C. Pietras, R.T. Pinker, K. Voss, and G. Zibordi, An emerging ground-based aerosol climatology: Aerosol optical depth from AERONET, *J. Geophys. Res.*, **106**, 12067-12097, 2001.

Huebert, B., T. Bates, P. Russell, G. Shi, Y.J. Kim, and K. Kawamura, An overview of

ACE-Asia: strategies for quantifying the relationships between Asian aerosols and their climatic impacts., *J. Geophys. Res.*, ACE-Asia special issue, submitted, 2003.

IPCC, *Climate Change 2001-The Scientific Basis* J. T. Houghton, Ed., Cambridge Univ. Press, 2001.

Jacobson, M. Z., Strong radiative heating due to the mixing state of black carbon in atmospheric aerosols, *Nature*, **409**, 695 - 697, 2001a.

Jacobson, M. Z., Global direct radiative forcing due to multicomponent anthropogenic and natural aerosols, *J. Geophys. Res.*, **106**, 1551-1568, 2001b.

Kaufman, Y. J., and T. Nakajima, Effect of Amazon smoke on cloud microphysics and albedo - Analysis from satellite imagery. *J. Appl. Meteor.*, **32**, 729-744, 1993.

Kaufman, Y.J., D. Tanre, O. Dubovik, A. Karnieli, and L.A. Remer, Absorption of sunlight by dust as inferred from satellite and ground-based remote sensing, *Geophys. Res. Lett.,* ***2*8**, 1479-1482, 2001.

Kawamoto, K., T. Nakajima, and T.Y. Nakajima, A global determination of cloud microphysics with AVHRR remote sensing, *J. Climate*, **14**, 2054-2068, 2001.

Kim, D.H., B.J. Sohn, T. Nakajima, and T. Takamura, Aerosol optical properties over East Asia determined from ground-based sky radiation measurements, *J. Geophys. Res.* , submitted, 2003.

Kinne, S., U. Lohmann, S. Ghan, R. Easter, M. Chin, P. Ginoux, T. Takemura, I. Tegen, D. Koch, M. Herzog, J. Penner, G. Pitari, B. Holben, T. Eck, A. Smirnov, O. Dubovik, I. Slutsker, D. Tanre, O. Torres, M. Mishchenko, I. Geogdzhayev, A. Chu, and Y.Kaufman, Monthly averages of aerosol properties: A global comparison among models, satellite data and AERONET ground data. *J. Geophys. Res.*, in press., 2002.

King, M.D., and B. M. Herman, Determination of the ground albedo and the index of absorption of atmospheric particulates by remote sensing. Part I: Theory, *J. Atmos. Sci.*, **36**, 163-173, 1979.

Menon, S., J. Hansen, L. Mazaranko, and Y. Luo, Climate effects of black carbon aerosols in China and India. , *Science*, **297**, 2250-2253, 2002.

Matsumoto, K., M. Uematsu, T. Hayano, K. Yoshioka, H. Tanimoto, and T. Iida, Simultaneous measurements of particulate elemental carbon on the ground observation network over the western North Pacific during the ACE-Asia campaign, *J. Geophys. Res.* , ACE-Asia special issue, submitted, 2003.

Nakajima, T., and M. Tanaka, Effect of wind-generated waves on the transfer of solar radiation in the atmosphere-ocean system, *J. Quant. Spectrosc. Radiat. Transfer*, **29**, 521-537, 1983.

Nakajima, T., and M. Tanaka, Matrix formulations for the transfer of solar radiation in a plane-parallel scattering atmosphere, *J. Quant. Spectrosc. Radiat. Transfer*, **35**, 13-21, 1986.

Nakajima, T., M. Tanaka, M. Yamano, M. Shiobara, K. Arao and Y. Nakanishi, Aerosol optical characteristics in the yellow sand events observed in May, 1982 in Nagasaki - Part II Model, *J. Meteor. Soc. Japan*, **67**, 279-291, 1989.

Nakajima, T., G. Tonna, R. Rao, Y. Kaufman, and B. Holben, Use of sky brightness measurements from ground for remote sensing of particulate polydispersions. *Appl. Opt.*, **35**, 2672-2686, 1996a.

Nakajima, T., T. Hayasaka, A. Higurashi, G. Hashida, N. Moharram-Nejad, Y. Najafi, and H. Valavi, Aerosol optical properties of Persian Gulf region Part I. Ground-based solar radiation measurements in Iran. *J. Appl. Meteor.*, **35**, 1265-1278, 1996b.

Nakajima, T., A. Higurashi, K. Kawamoto, and J. E. Penner, A possible correlation between satellitederived cloud and aerosol microphysical parameters, *Geophys. Res. Let.*, **28**, 1171-1174, 2001.

Nakajima, T. Y., and T. Nakajima, Wide-area determination of cloud microphysical properties from NOAA AVHRR measurements for FIRE and ASTEX regions, *J. Atmos. Sci.*, **52**, 4043-4059, 1995.

Nakajima, T. Y., A. Uchiyama, T. Takamura, and T. Nakajima, Inter comparisons of warm cloud properties obtained from satellite, aircraft, and ground equipments during APEX and ACE-Asia period in 2001, *J. Geophys. Res.*, ACE-Asia Special Issue, submitted, 2003.

Ohta, S., R. Kato, N. Murao, and S. Yamagata: Measruements of Optical and Chemical Properties of Atmospheric Aerosols at Fukue and Amami-Ohshima Islands. *J. Geophys. Res.*, ACE-Asia Specieal Issue, submitted, 2002.

Okada, I., T. Takamura , T. Inoue, and T.N. Nakajima, Development of a quasi real time system for estimate of the surface solar flux using GMS-5, SPIE's Third International Asia-Pacific Symposium on Remote Sensing of the Atmosphere, Environment, and Space, 23-27 October 2002,Dragon Hotel, Hagzhou, China, 2002.

Rajeev, K., and V. Ramanathan, Direct observations of clear-sky aerosol radiative

forcing from space during the Indian Ocean Experiment, *J. Geophys. Res.*, **106**, 17221-17235, 2001.

Ramanathan, V., P.J. Crutzen, J. Lelieveld, A.P. Mitra, D. Althausen, J. Andersen, M.O. Andreae, W. Cantrell, G.R. Cass, C.E. Chung, A.D. Clarke, J.A. Coalkey, W.D. Collins, W.C. Conant, F. Dulac, J. Heinzenberg, A.J. Heymsfield, B. Holben, S. Howell, J. Hudson, A. Jayaraman, J.T. Kiehl, T.N. Krishnamurti, D. Lubin, G. McFarquhar, T. Novakov, J.A. Ogren, I.A. Podgorny, K. Prather, K. Priestley, J.M. Prospero, P.K. Quinn, K. Rajeev, P. Rasch, S. Rupert, R. Sadourny, S.K. Satheesh, G.E. Shaw, P. Sheridan, and F.P.J. Valero, Indian Ocean Experiment: An integrated analysis of the climate forcing and effects of the great Indo-Asian haze, *J. Geophys. Res.*, **106**, 28371-28398, 2001.

Rossow, W. B., and L. C. Garder, Cloud detection using satellite measurements of infrared and visible radiances for ISCCP, *J. Climate*, **6**, 2341-2369, 1993.

Russell, P.B., J. M. Livingston, P. Hignett, S. Kinne, J. Wong, A. Chien, R. Bergstrom, P. Durkee and P. V. Hobbs, Aerosol-induced radiative flux changes off the United States mid-Atlantic coast: Comparison of values calculated from sunphotometer and in situ data with those measured by airborne pyranometer, *J. Geophys. Res.*, **104**, 2289-2307, 1999.

Saito, K., and T. Kato, The MRI mesoscale nonhydrostatic model. *Met. Res. Note*, **196**, 169-195, 1999 (in Japanese).

Sekiguchi, M., T. Nakajima, K. Suzuki, K. Kawamoto, A. Higurashi, D. Rosenfeld, I. Sano, and S. Mukai, A study of the direct and indirect effects of aerosols using global satellite datasets of aerosol and cloud parameters, *J. Geophys. Res.*, 2003, under revision.

Shimizu, A., N. Sugimoto, I. Matsui, K. Arao, T. Murayama, N. Kagawa, and I. Uno, Continuous observations of Asian dust and other aerosols by dual-polarization lidars in China and Japan during ACE-Asia, *J. Geophys. Res.*, ACE-Asia Special Issue, submitted, 2003.

Tanaka, M., T. Takamura and T. Nakajima, Refractive index and size distribution of aerosols as estimated from light scattering measurements, *J. Climate Appl. Meteor.*, **22**, 1253-1261, 1983.

Tanaka, M., T. Nakajima, and M. Shiobara, Calibration of a sunphotometer by simultaneous measurements of direct-solar and circumsolar radiations. *Appl. Opt.*,

25, 1170-1176, 1986.

Takemura, T., H. Okamoto, Y. Maruyama, A. Numaguti, A. Higurashi, and T. Nakajima, Global three-dimensional simulation of aerosol optical thickness distribution of various origins, *J. Geophys. Res.*, **105**, 17853-17873, 2000.

Takemura, T., T. Nakajima, T. Nozawa, and K. Aoki, Simulation of Future Aerosol Distribution, Radiative Forcing, and Long-range Transport in East Asia, *J. Meteor. Soc. Japan,* 79, 1139-1155, 2001.

Takemura, T., T. Nakajima, O. Dubovik, B. N. Holben, and S. Kinne, Single scattering albedo and radiative forcing of various aerosol species with a global three-dimensional model. *J. Climate*, **15**, 333-352, 2002a.

Takemura, T., I. Uno, T. Nakajima, A. Higurashi, and I. Sano, Modeling study of long-range transport of Asian dust and anthropogenic aerosols from East Asia. *Geophys. Res. Lett.*, **29**, 2158, doi:10.1029/2002GL016251, 2002b.

Takemura, T., T. Nakajima, A. Higurashi, I. Sano, S. Ohta, N. Sugimoto, T.L. Anderson, and S.J. Masonis, Aerosol distributions and radiative forcing over the Asian-Pacific region simulated by the SPRINTARS, *J. Geophys. Res.*, ACE-Asia Special Issue, submitted, 2003.

Uematsu, M., A. Yoshikawa, H. Muraki, K. Arao, and I. Uno, Transport of mineral and anthropogenic aerosols during a Kosa event over East Asia, *J. Geophys. Res.*, **107**, AAC3/1-7, 2002.

Uno, I., G.R.Carmicahel, D.G. Streets, Y.Tang, J.J.Yienger, S.Satake, Z.Wang, Jung-Hun Woo, S.Guttikunda, M.Uematsu, K. Matsumoto, H.Tanimoto, K.Yoshioka and T. Iida, 2002: Regional chemical weather forecasting using CFORS: Analysis of surface observations at Japanese Island stations during the ACE-Asia Experiment, *J. Geophys. Res.*, submitted, 2003.

WCP(World Climate Programme), Report of the experts meeting on aerosols and their climatic effects, Williansburg, Virginia, 28-30 March 1983, edited by Deepak, A. and H. E. Gerber, WMO-ICSU, WCP-55, 1983.

Table 1. Location and instrumentation at sites in the target region.

Site	Location	Program	Instrumentation
Hefei	31.78N, 117.30E	SKYNET	radiometers, skyradiometer, lidar, microwave radiometer, absorptionmeter, nephelometer
Qingdao	36.26N, 120.38E	ADEC	lidar
Anmyondo	36.50N, 126.30E	SNU	radiometers, skyradiometer
Gosan	33.28N, 127.17E	KMA/ ACE-Asia	radiometers, skyradiometer, Cimel sun photometer, lidar absorption meter, nephelometer, aerosol sampling
Miyakojima	24.76N, 125.28E	JMA/ SKYNET	skyradiometer, (radiometer, absorption meter, nephelometer)
Naha	26.21N, 127.68E	ADEC	skyradiometer, lidar
Amami-Oshima	28.15N, 129.30E	SKYNET	radiometers, skyradiometer, lidar, microwave radiatometer, absorption meter, nephelometer, aerosol sampling
Fukuejima	32.70N, 128.85E	SKYNET	(radiometers, skyradiometer, lidar, microwave radiatometer, absorption meter, nephelometer, aerosol sampling)
Shiraharam	33.63N, 135.41E	AERONET	Cimel sun photometer
Mineyama	35.57N, 135.05E	AERONET	Cimel sun photometer, radiometer, absorption meter, nephelometer, aerosol sampling
Hachijojima	33.13N, 139.74E	VMAP	aerosol sampling
Sado	38.00N, 138.40E	VMAP	aerosol sampling
Rishiri	45.20N, 141.25E	VMAP	aerosol sampling

* KMA: Korean Meteorological Agency; JMA: Japan Meteorological Agency; SNU: Seoul National University; Instruments in parentheses operated since 2002.

Table 2. Monthly mean values of aerosol and cloud parameters and radiative forcings at Gosan and Amami-Oshima sites. April 2001 results.

	Gosan				Amami			
Quantity	CFORS	SPRINTARS	Satellite	Surface	CFORS	SPRINTARS	Satellite	Surface
τ_{500}	0.305	0.371	0.443	0.413	0.334	0.348	0.385	0.390
(rmsd)	0.154	0.177	0.184	0.116	0.128	0.139	0.171	0.126
ω_{500}	0.922	0.935	0.903	0.919	0.934	0.957	0.935	0.861
(rmsd)	0.017	0.022	0.038	0.056	0.015	0.009	0.032	0.062
g_{500}	0.720	0.710	0.674	0.705	0.719	0.712	0.711	0.685
(rmsd)	0.020	0.012	0.024	0.036	0.025	0.015	0.035	0.034
ARF(SW,clr,toa)	-7.89	-10.55	-11.47	-10.47	-8.49	-10.15	-10.29	-7.50
(rmsd)	3.75	5.04	3.93	4.50	3.36	3.92	3.59	4.49
ARF(SW,clr,sfc)	-19.82	-21.55	-30.66	-25.92	-19.16	-17.62	-23.49	-31.08
(rmsd)	10.96	7.77	11.80	8.29	7.12	6.24	12.82	8.80
CRF(tot,toa)	-20.95	-19.73	-18.09	-	-36.57	-36.17	-36.50	-
CRF(tot,sfc)	-19.33	-18.71	-15.67	-	-34.42	-34.86	-33.00	-
ARFD(tot,all,toa)	-4.98	-6.84	-8.24	-8.21	-5.08	-6.20	-6.62	-4.60
ARFD(tot,all,sfc)	-12.52	-13.71	-23.94	-22.48	-12.26	-10.26	-15.62	-25.21
ARFI(tot,all,toa)	-	-0.35	-0.86	-	-	-1.62	-1.56	-
ARFI(tot,all,sfc)	-	-1.55	-1.30	-	-	-3.40	-1.13	-

Table 3 Mean and RMSD values of cloud amount (n) and cloud optical thickness (τ) at Gosan and Amami-Oshima in April 2001. Values for low (L), middle (M), and high (H) level clouds are shown.

Site	n_L	n_M	n_H	τ_L	τ_M	τ_H
Gosan	14.7	17.5	16.0	6.9	8.6	5.9
(rmsd)	27.1	26.2	21.9	6.8	8.1	8.0
Amami	22.7	17.4	14.1	13.5	10.0	5.4
(rmsd)	34.8	24.7	19.8	10.2	10.1	3.2

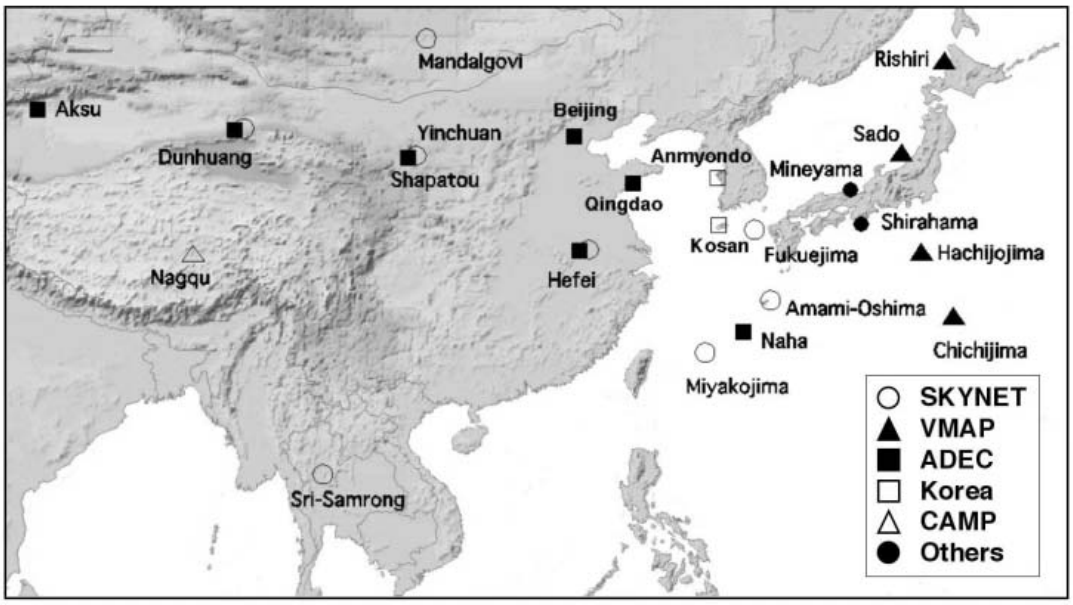

Figure 1. Asian radiation and aerosol measurement sites.

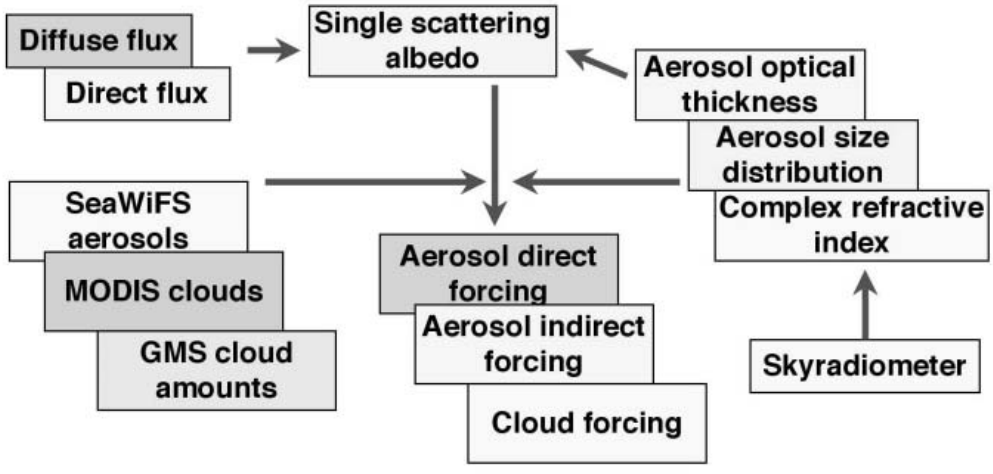

Figure 2. Schematic diagram for deriving aerosol and cloud radiative forcings.

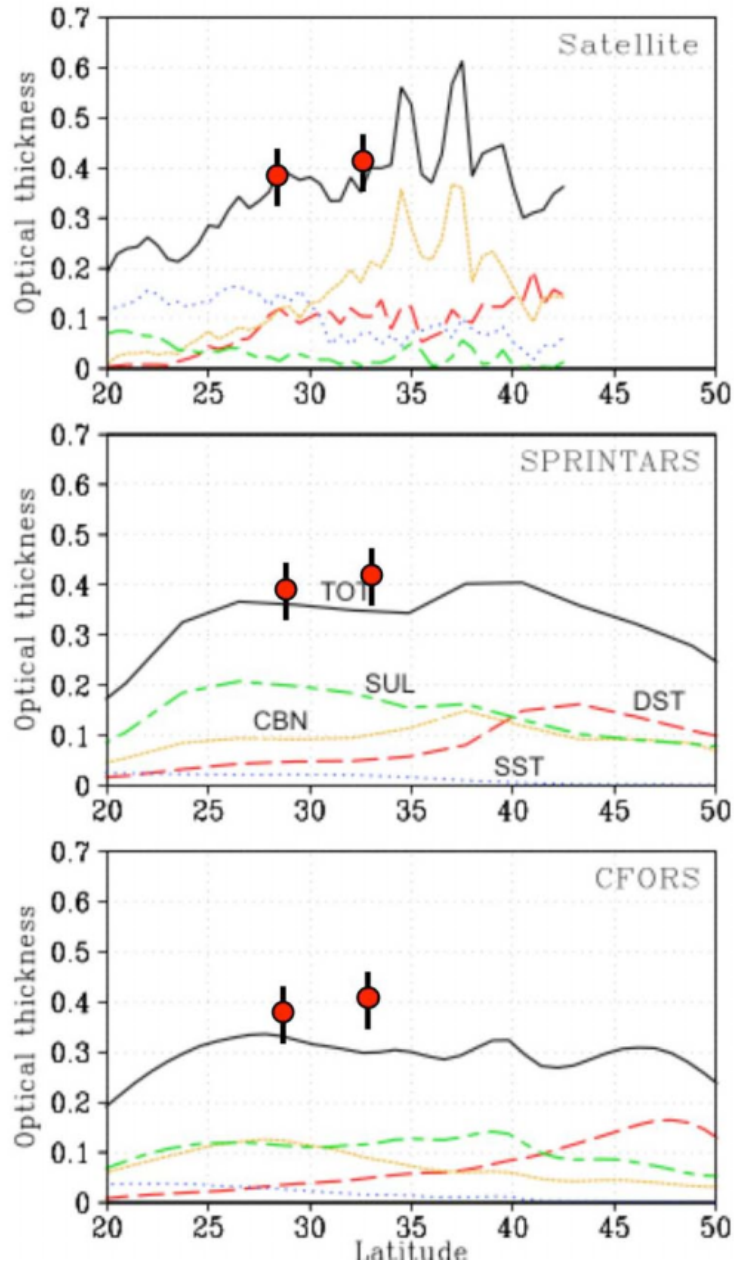

Figure 3. April monthly mean AOT values averaged in the longitude belt between 125.5E and 130.5E as a function of latitude for sulfate (SUL), carbonaceous (CBN), mineral dust (DST), and sea salt (SLT) aerosols derived from CFORS and SPRINTARS model simulations and SeaWiFS remote sensing are shown. The total AOT from the various methods (thick solid lines) and surface methods (circles) are also shown.

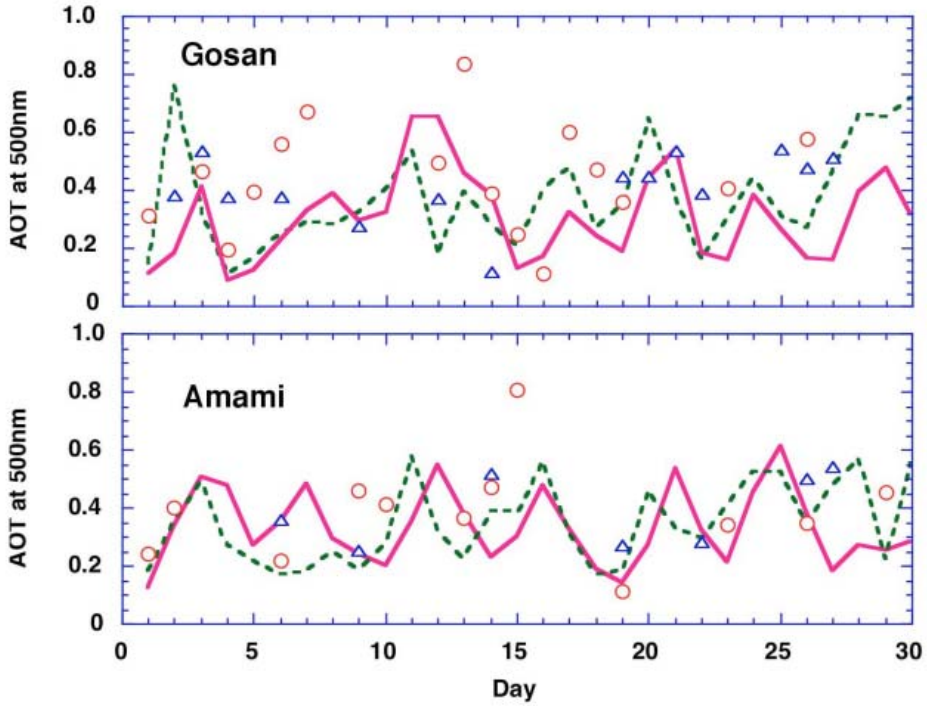

Figure 4. Time series of AOT as a function of day in April 2001 at Gosan and Amami-Oshima sites. Results from CFORS (solid line), SPRINTARS (broken line), satellite (circles), and surface method (triangles).

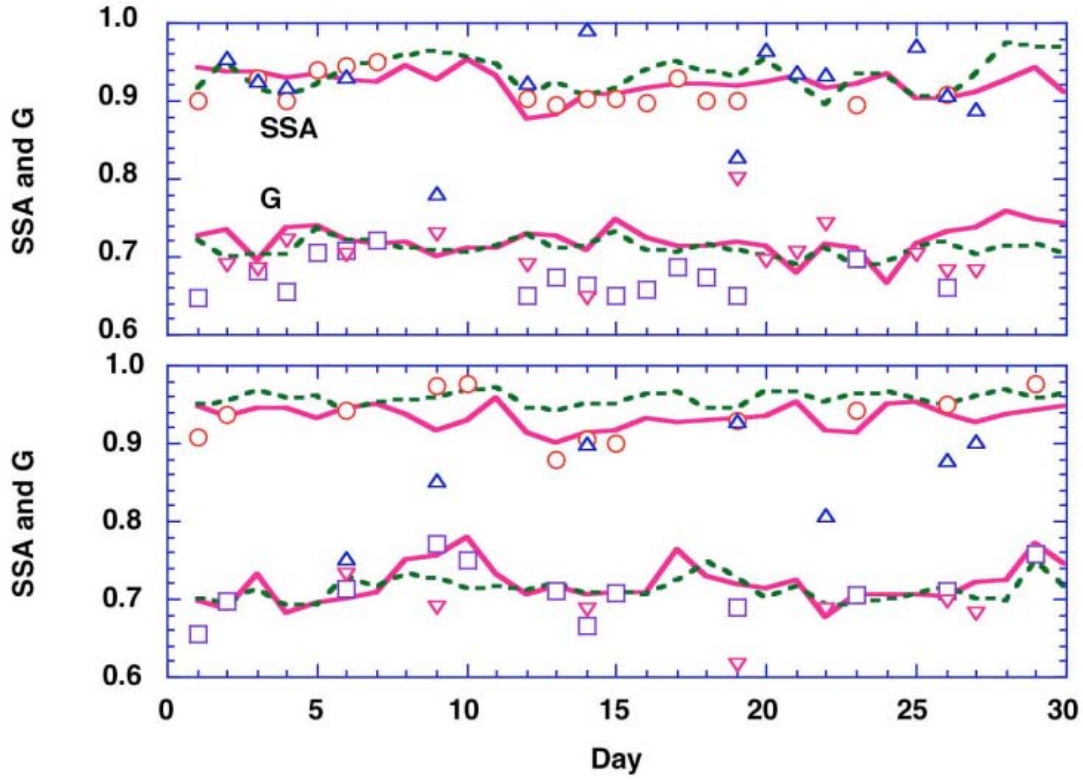

Figure 5. Same as in Fig.4 but for single scattering albedo and asymmetry factor. Results from CFORS (solid lines), SPRINTARS (broken lines), satellite (circles and squares), and surface method (triangles).

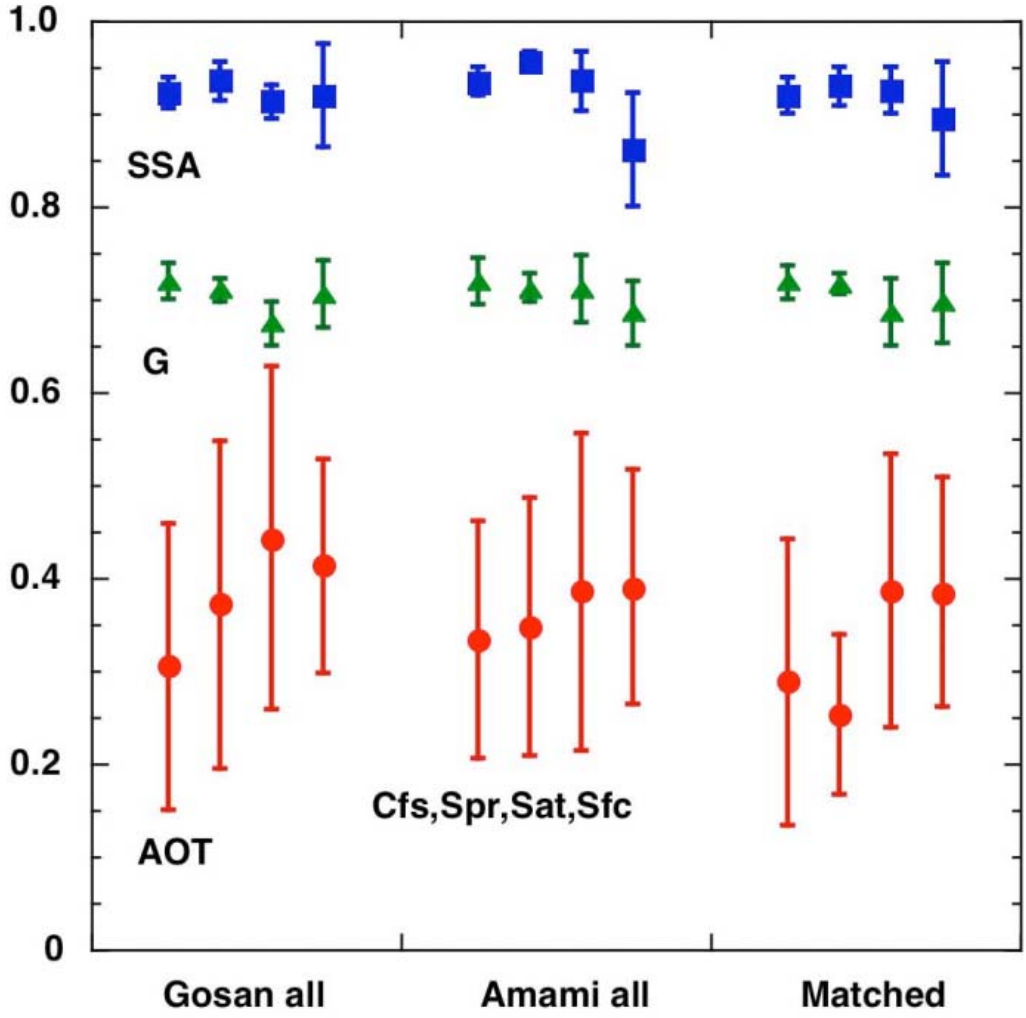

Figure 6. Comparison of AOT, SSA, and asymmetry factor at Gosan and Amami-Oshima as averages of daily values of April 2001. We also compare averages calculated from data on 11 days at Gosan and 6 days at Amami-Oshima when all the methods are available as labeled 'Matched'.

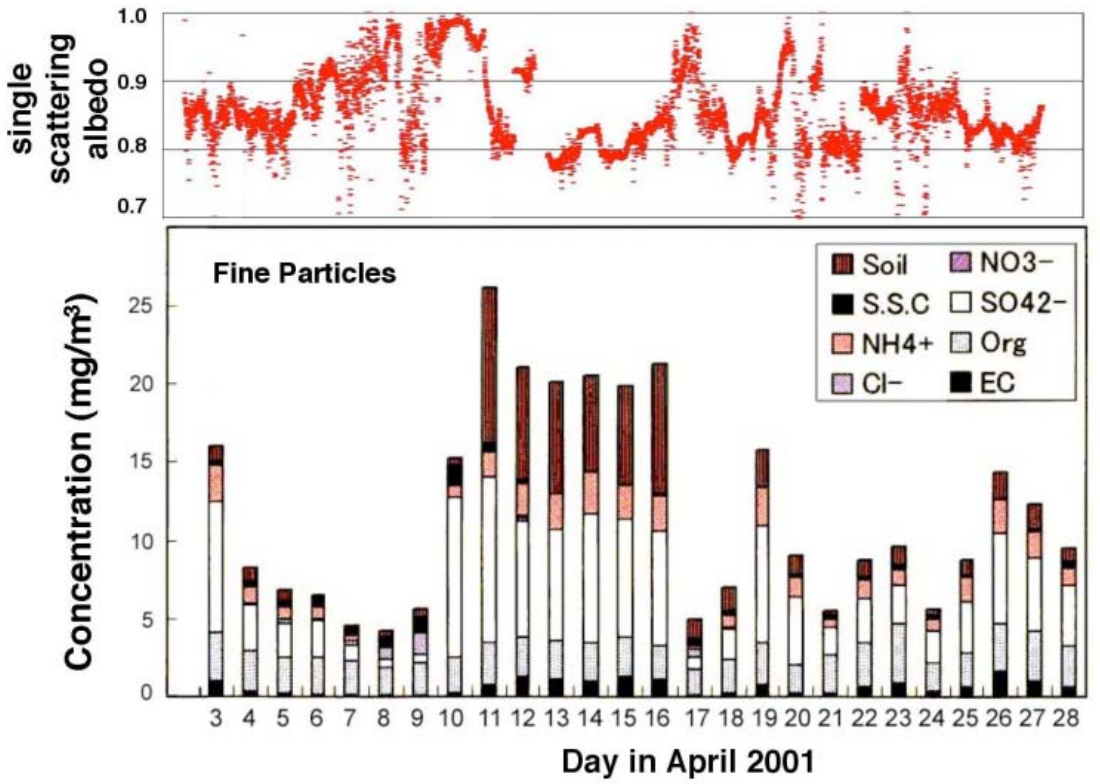

Figure 7. Time series of aerosol single scattering albedo and chemical composition of particles with radius less than 1 μm measured at Amami-Oshima site in April 2001.

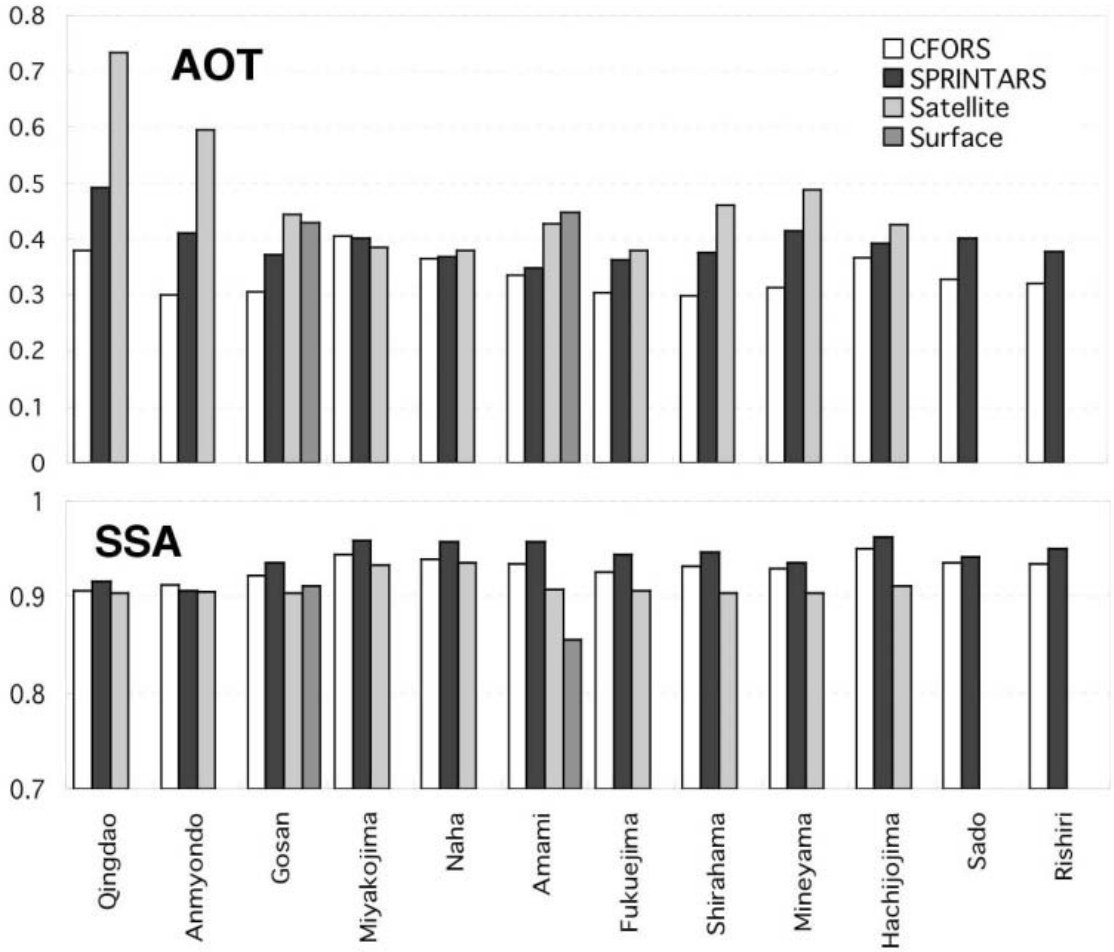

Figure 8. AOT and SSA at 500nm evaluated at sites in Table 1 by various methods.

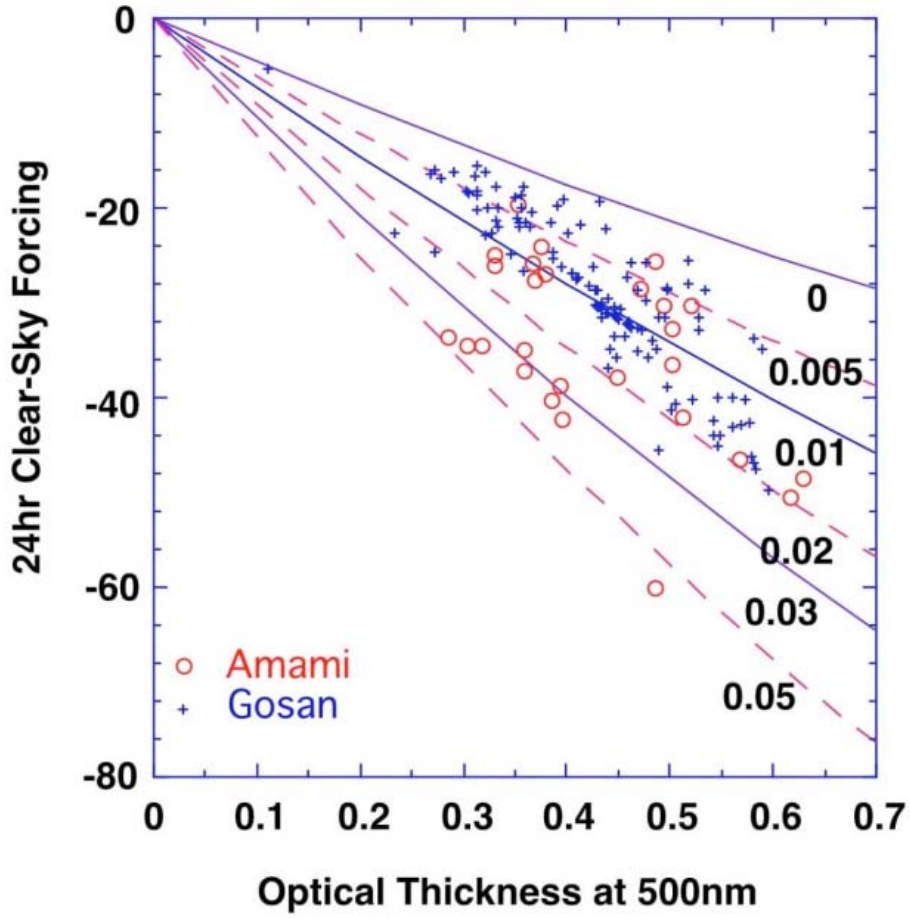

Figure 9. The 24 hour mean clear sky net shortwave ARF as a function of AOT at 500nm at Gosan and Amami-Oshima. Theoretical values with Junge aerosol size distribution and US standard amosphere are also presented as a reference. The imaginary part of the aerosol refractive index are changed from 0 to -0.05 as labeled.

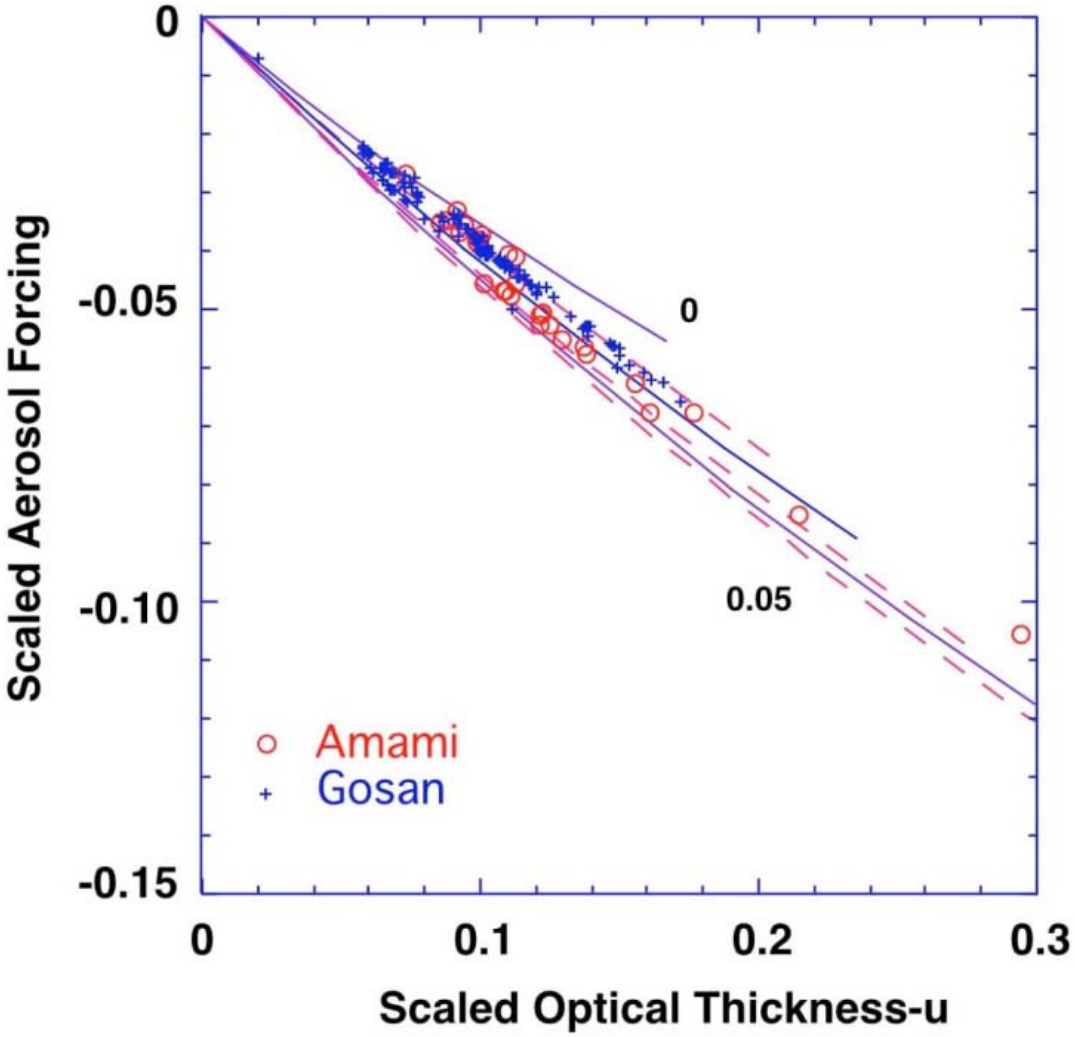

Figure 10. Same as in Fig. 8 but for scaled ARF and optical thikcness.

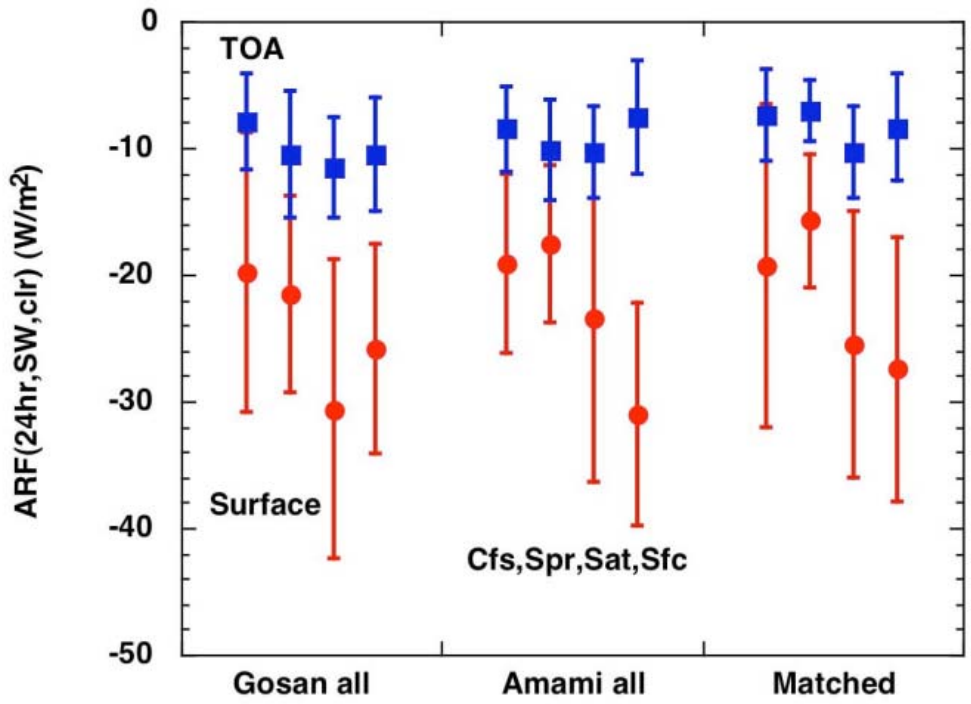

Figure 11. The 24 hour clear sky net shortwave ARF at Gosan and Amami-Oshima.

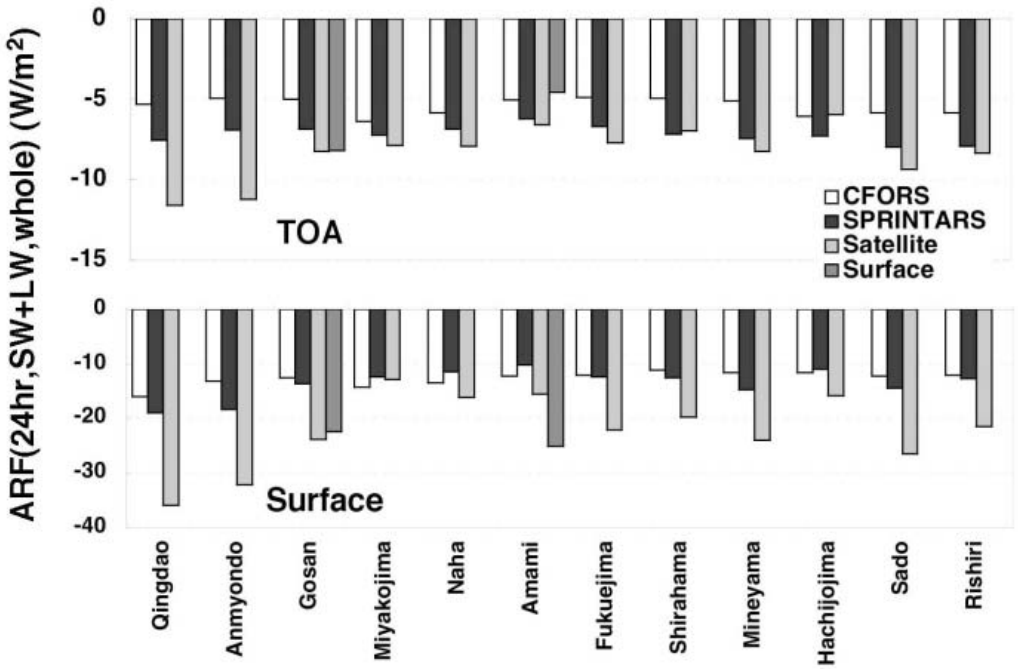

Figure 12. Whole sky radiative forcings (W/m^2) evaluated by the various methods at sites listed in Table 1. Shortwave clear sky forcings at Gosan and Amami-Oshiam are also compared. Monthly mean of April 2001.

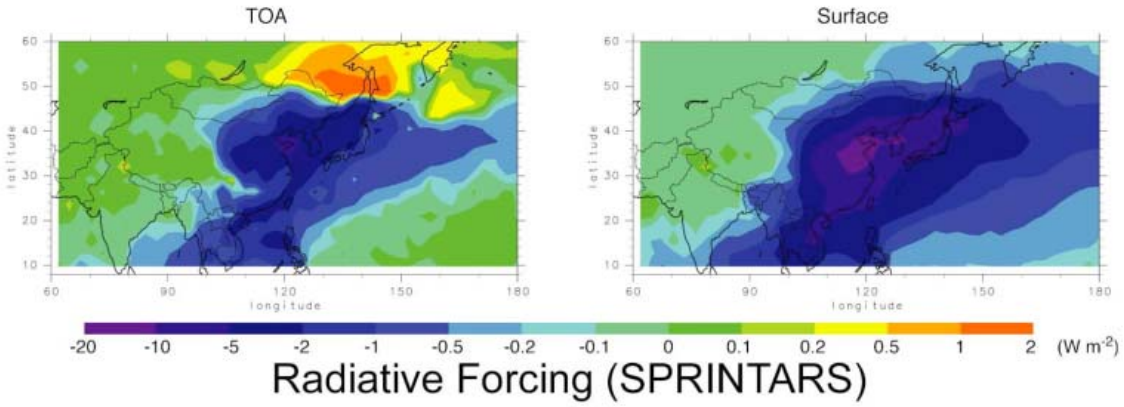

Figure 13. Distributions of the aerosol direct radiative forcings (W/m^2) at TOA and surface calculated by SPRINTARS model. Monthly mean of April 2001.

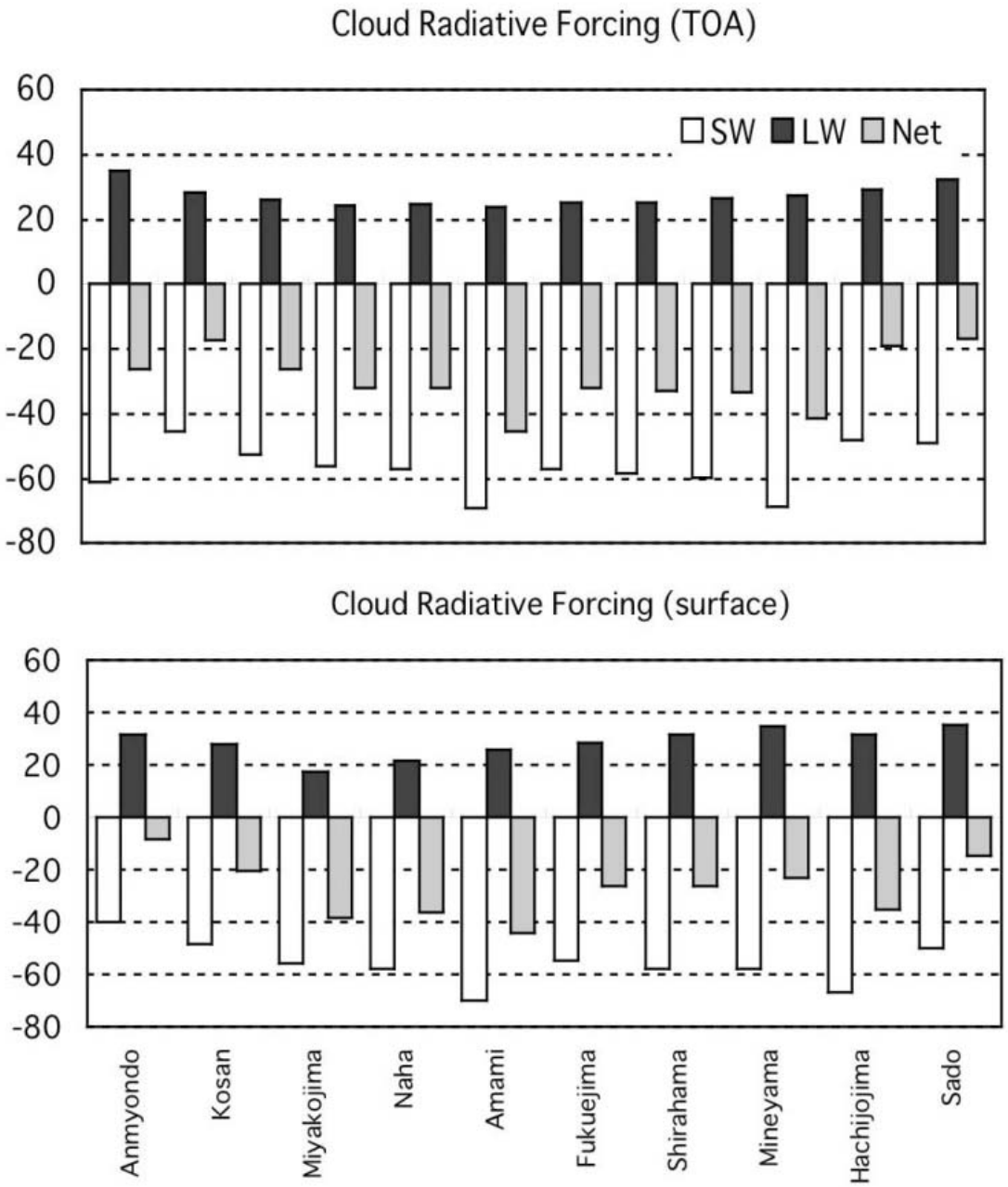

Figure 14. Cloud radiative forcings (W/m^2) at TOA and surface. Montly mean of April 2001.

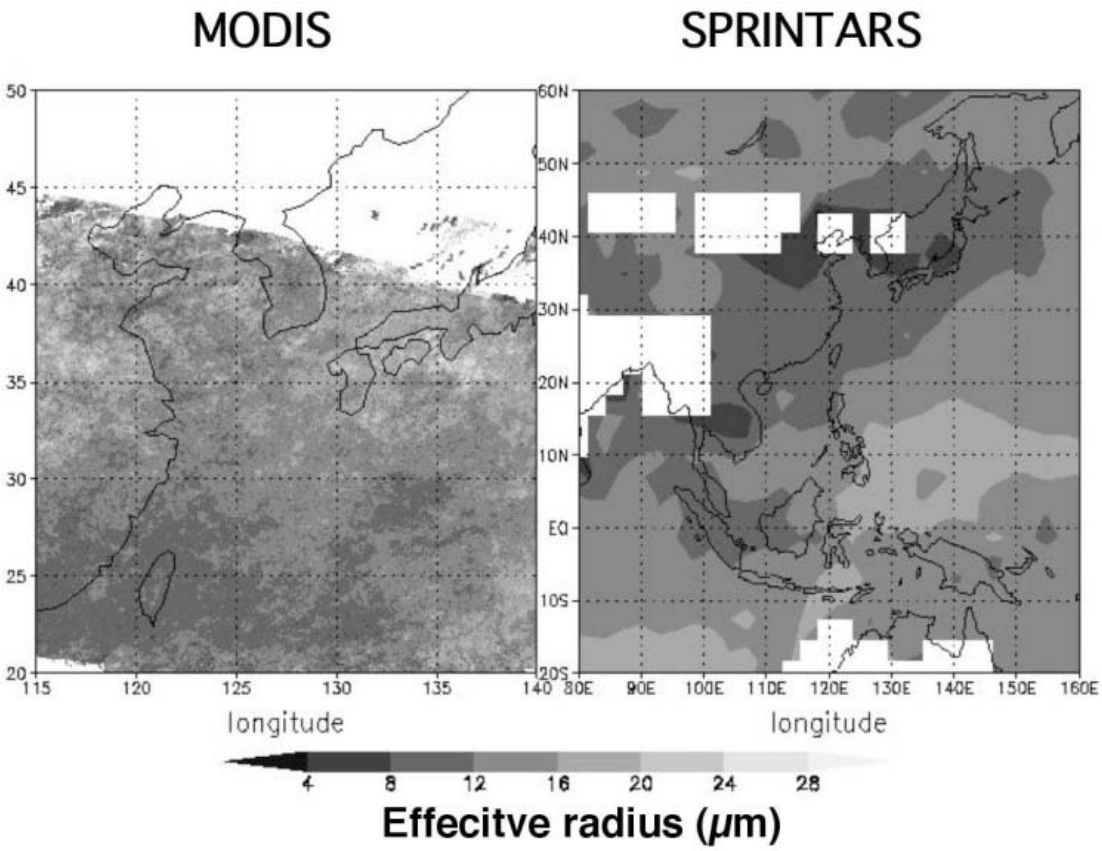

Figure 15. Distributions of the effective cloud particle radius (μm) from MODIS retrievals and SPRINTARS model simulation. Monthly mean of April 2001.

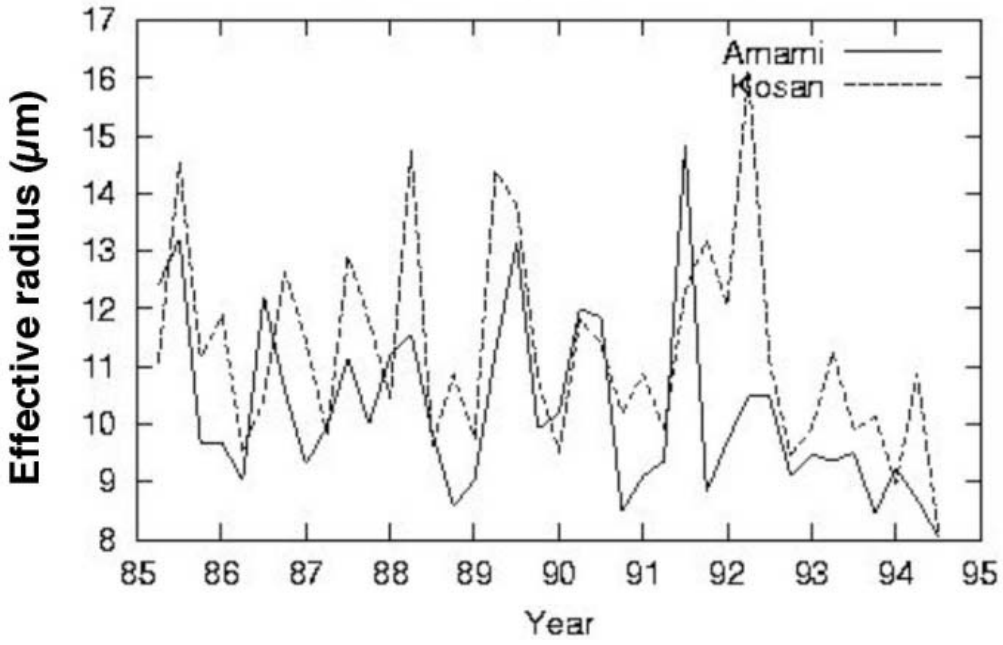

Figure 16. Time series of the effective particle size obtained from AVHRR retrieval.

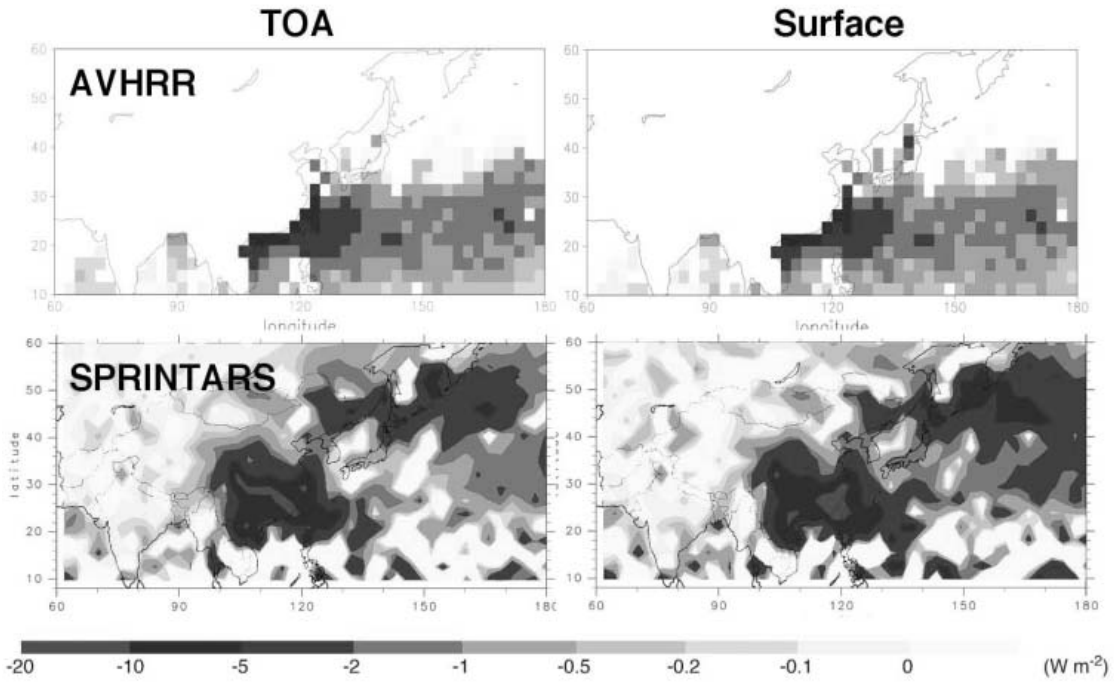

Figure 17. Distributions of the indirect forcing of man-made aerosols (W/m^2) evaluated by AVHRR and by SPRINTAR model. See the text for derivation method.

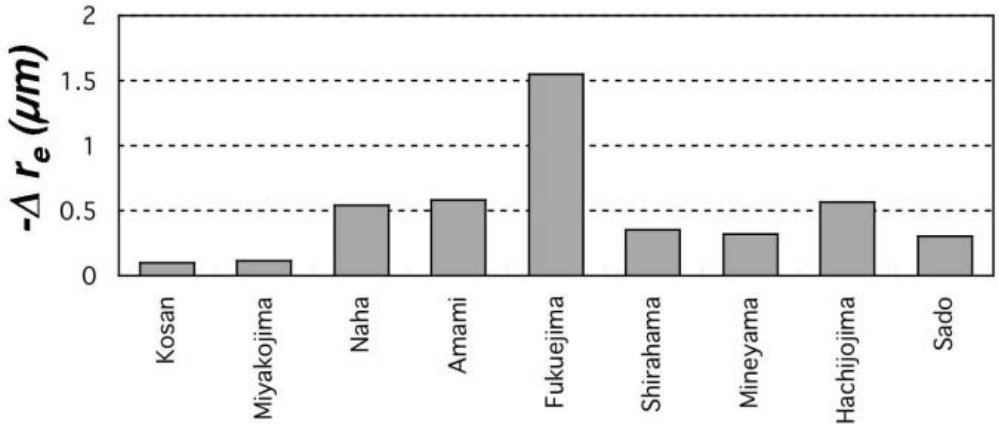

Figure 18. Magnitude of reduction in the effective particle radius of low level cloud due to 30% increase in the column aerosol particle number evaluated by AVHRR retrieval. April monthly mean of 1990.

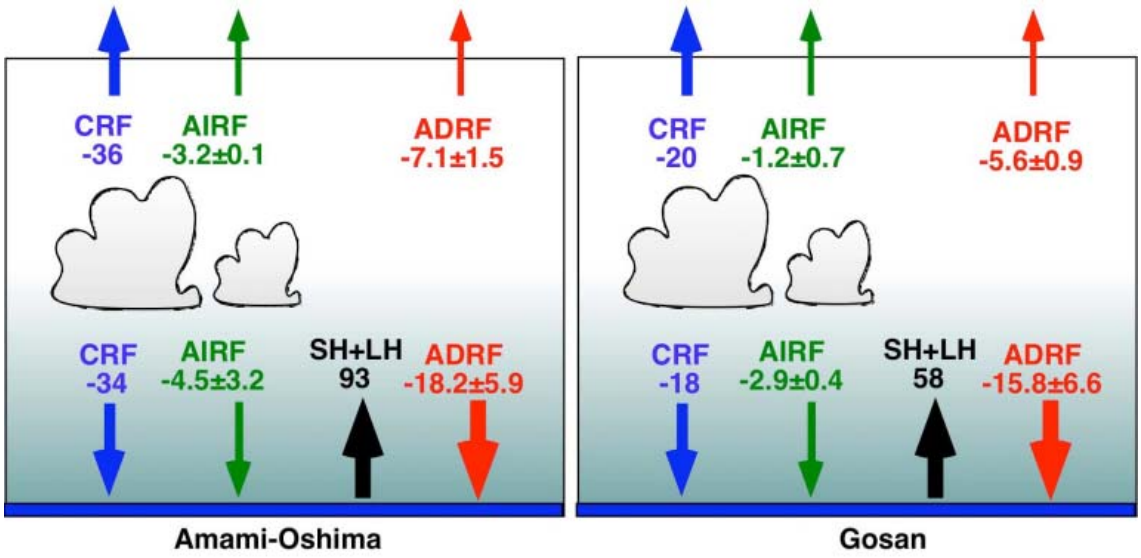

Figure 19. Monthly mean aspects of the radiation budget at Gosan and Amami-Oshima sites in April 2001. Whole sky aerosol direct forcing (ADRF), indirect forcing (AIRF), cloud radiative forcing (CRF), and sensible and latent heat flux (SH+LH) are shown as monthly mean values in April 2001.